Use of dissolved hyperpolarized species in NMR: practical considerations

Patrick Berthault [a,*], Céline Boutin [a], Charlotte Martineau-Corcos [c], Guillaume Carret [b]

[a]NIMBE, CEA, CNRS, Université Paris-Saclay, CEA Saclay 91191 Gif-sur-Yvette, France

[b]Cortecnet, 15 rue des tilleuls, 78960 Voisins-le-Bretonneux, France

[c]ILV, UMR CNRS 8180, Université de Versailles Saint Quentin, 45 avenue des Etats-Unis, 78035 Versailles Cedex, France

Edited by Gareth Morris and Geoffrey Bodenhausen

Abstract

Hyperpolarization techniques that can transiently boost nuclear spin polarization are generally carried out at low temperature - as in the case of dynamic nuclear polarization - or at high temperature in the gaseous state - as in the case of optically pumped noble gases. This review aims at describing the various issues and challenges that have been encountered during dissolution of hyperpolarized species, and solutions to these problems that have been or are currently proposed in the literature. During the transport of molecules from the polarizer to the NMR detection region, and when the hyperpolarized species or a precursor of hyperpolarization (e.g. parahydrogen) is introduced into the solution of interest, several obstacles need to be overcome to keep a high level of final magnetization. The choice of the magnetic field, the design of the dissolution setup, and ways to isolate hyperpolarized compounds from relaxation agents will be presented. Due to the non-equilibrium character of the hyperpolarization, new NMR pulse sequences that perform better than the classical ones will be described. Finally, three applications in the field of biology will be briefly mentioned.

Keywords: Hyperpolarization; Optical pumping; Dynamic Nuclear Polarization; Parahydrogen

1 Introduction

Production of spin–hyperpolarized species for enhancing NMR sensitivity is nowadays becoming routine. Whatever the hyperpolarization method chosen - let us cite here the three main methods: Dynamic Nuclear polarization (DNP), Para-Hydrogen Induced Polarization (PHIP), and Optical Pumping (OP) - all of these techniques have largely been documented, and high polarization levels (typically from 5% to 90%) are easily reached. But in our opinion the challenge is now elsewhere, and can be separated into two points : i) finding the best way to deliver hyperpolarized species in solution, by maximizing their concentration and obtaining a high and reproducible magnetization (which is proportional to the product of concentration and polarization); and ii) taking best advantage of the transient character of the hyperpolarization by developing fast NMR/MRI pulse sequences.

The development of on-line hyperpolarization methods is not exempt from such concerns. They are also susceptible to problems linked to pollution by substances required during the production of the hyperpolarization, for instance traces of alkali metal from spin–exchange

optical pumping (SEOP) can be deposited all along the transfer line to the mixing chamber. For polarization by addition of parahydrogen, the hydrogenation catalyst can be difficult to separate from the molecules of interest. For dissolution-DNP, there can be poor separation of the molecule of interest from the components of the glassy matrix containing the free radicals.

This review is primarily conerned with the challenges of delivering high polarizations in aqueous solution. These are particularly severe where the hyperpolarized species (or its precursor) is hydrophobic: for example xenon is only soluble in water at 4.5 mM per bar at 20°C, di-hydrogen at 0.6 mM per bar.[1]

Although there are some common factors, procedures for handling hyperpolarized substances differ according to their mode of production. In order to avoid severe polarization losses, hyperpolarized xenon has to stay in a significant magnetic field (typically at least on the order of 10 mT). In order to achieve efficient polarization transfer in some parahydrogen experiments, the magnetic field has to be precisely controlled. In contrast for the survival of the parahydrogen, the enrichment itself does not require a magnetic field, as the conversion rate between parahydrogen (singlet state) and ortho-hydrogen (triplet state) is determined by dipolar relaxation, *e.g.,* by the presence of paramagnetic impurities inside the reservoir.[2]

The problems are even more severe if biological material is under study, as the constraints imposed by hyperpolarization are exacerbated by those related to cell survival or, biological tissue or animal handling.

This review describes various devices that allow delivery of hyperpolarized species in solution, in cell suspensions, or in fixed/perfused biological tissues. In no case does it aim to be exhaustive, and some subjectivity may be discernible in the discussion part. In the discussion that follows, we will firstly ask ourselves why there is such a tremendous need for hyperpolarized species, since an objective consideration would necessarily take into account the high ratio of the time required for their preparation to the actual NMR experiment time, which can make hyperpolarization uncompetitive. Secondly we will detail the difficulties associated with optimal use of hyperpolarized species in liquid state NMR. Thirdly we will focus on the necessarily incomplete state of the art of existing experimental setups. As instrumentation is of little value unless it is paired with powerful methodology, we will insist on combining fast NMR pulse sequences with the devices delivering hyperpolarization in solution. We will finally describe some applications in the field of biology.

2 Why do we need hyperpolarized species ?

The first answer may seem obvious, but the tremendous gain in NMR signal *per se* is not always the most important thing. Sometimes it is the resulting selectivity that matters most. This selectivity is usually afforded by the low concentration of the hyperpolarized species (and therefore its high detectability). Think for instance of the area of ^{129}Xe NMR-based biosensing, of which two examples are provided below. The strength of this approach lies in the high responsiveness of xenon to its local environment, which - due to the high deformability of the electron cloud of this atom - translates into wide variation in NMR parameters such as chemical shifts and relaxation times. This property has in particular been used to develop molecular systems designed to reversibly encapsulate xenon and give it a specific resonance frequency. As these molecular systems can be decorated by ligands bearing biological receptors,^{129}Xe spectroscopic imaging can enable localization of the latter.

In this research area, the use of hyperpolarized xenon is mandatory for the following reasons, in addition to the need for sensitivity enhancement :

- If the binding constant for xenon encapsulation is to be measured accurately, the receptor sites of the host molecule must be only partly occupied. The highest accuracy in such measurements will be reached when the concentration of dissolved xenon is comparable to that of the host molecule. Considering for instance the case of some cryptophanes, which have long been recognized as good candidates for ^{129}Xe NMR-based biosensing, the difficulty of their synthesis means that large concentrations are not easily available. Therefore it is important to be able to characterize the thermodynamic and kinetic aspects of their interaction with low quantities of xenon.
- If one wishes to discriminate beween multiple probes through their different xenon resonance frequencies, as illustrated in Figure 1, because of the so-called kick-out or degenerate exchange mechanism, in which a caged xenon atom is expelled by another xenon,[3, 4, 5] the lifetime of caged xenon is shortened when the noble gas concentration increases, and therefore the signal of xenon in the host molecule is broadened. Better spectral discrimination is achieved with low xenon concentrations.

These two examples in the field of ^{129}Xe NMR-based biosensing show that it can be mandatory to work with concentrations of xenon adapted to the sample of interest and reproducible degrees of hyperpolarization. As a consequence, the best polarization system is one which

delivers not only a high polarization level, but also a controlled concentration of hyperpolarized species.

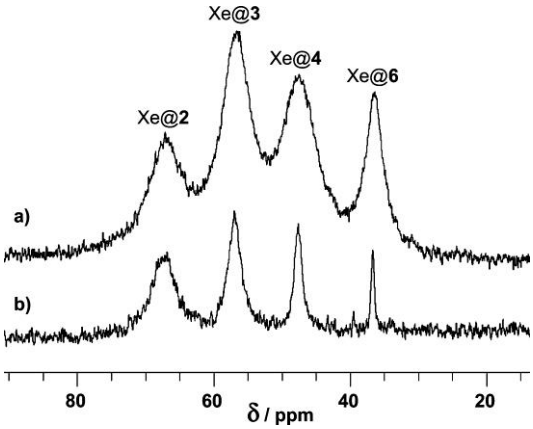


Figure 1: High-field region of the laser-polarized ^{129}Xe NMR spectrum of an aqueous solution of four cryptophanes at millimolar concentration, under xenon pressures of (a) 1.6×10^5 Pa, and (b) 3×10^4 Pa. Reprinted with permission from ref. [3].

3 What are the difficulties associated with dissolution of hyperpolarized species ?

In order to use hyperpolarized species in liquid-state NMR, it is often necessary to dissolve them in the solution of interest, since they are prepared in the polarizer in a different physical state: either gaseous, for noble gases or parahydrogen, or embedded in a glassy matrix containing radicals, in the case of DNP. The aspects that are important here are thus maximizing recovery of the hyperpolarized species, and minimizing relaxation during transport to the NMR spectrometer (including extraction from the polarizer) and during dissolution in the sample of interest. In each of these steps relaxation will occur, more or less efficiently. In addition, the transfer steps may not be quantitative, causing loss of some of the hyperpolarized species. These two effects need to be controlled in order to ensure a reproducible process, in which both the amount of the hyperpolarized species in solution and its polarization are stable. Depending on the state of the hyperpolarized compounds and/or the accompanying magnetic field, the problems with maintaining polarization can be very different. Below, we discuss separately the two steps required, transport from the polarizer to the NMR magnet (sometimes via storage), and the dissolution step.

3.1 Depolarization between the polarizer and the NMR magnet

3.1.1 Optically-pumped noble gases

^{129}Xe and ^{83}Kr

In the case of Spin Exchange Optical Pumping devices, the hyperpolarized species are noble gases such as ^{3}He , ^{129}Xe or ^{83}Kr, mixed with alkali metal vapors and buffer gases such as nitrogen or helium needed to perform hyperpolarization. Classically, nitrogen is used to quench radiative de-excitation, and helium serves to increase the pressure in the pumping cell in order to match the width of the metal atom absorption line to the emission bandwidth of the laser diode. After optical pumping, the retrieval of the hyperpolarized atoms therefore consists in the extraction of the gas volume from the polarizer, followed by separation and concentration steps to prepare them for transport. A convenient way to transport the polarized noble gas is to condense it to a solid. Due to their respective triple points of 115.8 K and 161.4 K, krypton and xenon can be efficiently condensed and frozen using easily handled cryogenic fluids such as liquid nitrogen.

However the noble gas T_1(^{129}Xe) and T_1(^{83}Kr) have been shown by Happer *et al.* to depend strongly on magnetic field.[6] In the gas phase, relaxation is accelerated in the presence of magnetic field gradients (through variations of the orientation rather than the magnitude of the local fields).[7] In the gas phase, the ^{129}Xe longitudinal relaxation rate can be expressed as:

$$\frac{1}{T_1^{Xe}} = \frac{1}{T_1^{sr}} + \frac{1}{T_1^{dd}} + \frac{1}{T_1^{w}} + \frac{1}{T_1^{D}}$$

where $\frac{1}{T_1^{sr}}$ is the spin-rotation relaxation term linked to collisions (which decreases with temperature and xenon concentration), $\frac{1}{T_1^{dd}}$ stands for dipole-dipole relaxation with free paramagnetic species such as O_2, $\frac{1}{T_1^{w}}$ is also dipolar, arising from paramagnetic sites in the container wall, and $\frac{1}{T_1^{D}}$ reflects relaxation through diffusion in inhomogeneous magnetic fields.[8]

While the second term can easily be minimized, the third and fourth terms need special care. For relaxation at the container wall, the volume to surface ratio can be maximized, but, more importantly, applying a monolayer coating of a suitable siloxane-type preparation to the

container walls gives a significant lengthening of the noble gas longitudinal relaxation time.[9, 10, 11] Relaxation by diffusion in an inhomogeneous field is governed by the equation:

$$\frac{1}{T_1^D} = \frac{|\overrightarrow{\nabla\Omega_\perp}|^2 D}{\omega^2}$$

where D is the diffusion coefficient, $\nabla\Omega_\perp$ is the Larmor precession frequency due to the transverse components of the derivatives of magnetic field intensity, and ω is the ^{129}Xe Larmor frequency.[6] Therefore the best situation would be an intense and homogeneous magnetic field. The depolarization problem is even more severe when xenon changes state (from gas to solid or vice versa), as a further relaxation term arises from interactions with phonons in the crystal; a magnetic field of several tenths of Tesla is therefore required during this step.[12, 13]

The case of ^{83}Kr deserves particular mention. Hyperpolarized ^{83}Kr, used as a probe of surfaces, mainly by the group of T. Meersmann,[14, 15, 16] is a special case as it is a quadrupolar nucleus. While it has been shown in the gas phase to constitute a powerful probe of surface-to-volume ratio changes through quadrupolar relaxation contrast (the SQUARE approach, which has been applied for instance in an animal model of emphysema,[17]), few studies have dealt with its use in the dissolved state even though its chemical shift behaviour as a function of solvent is strongly correlated with that of ^{129}Xe. Mazitov *et al.* [18] found the following relationship, in ppm :

$$\delta\left(^{129}Xe\right) = 1.8 \times \delta\left(^{83}Kr\right) + 15.5$$

Thus in the dissolved state it could be interesting to compare two noble gases with similar physical properties that differ mostly in their atomic size.

Whatever the application, maintaining the hyperpolarization of ^{83}Kr as it is transported from the optical pumping cell containing paramagnetic alkali metal vapor to the NMR detection area is not straightforward. As the cryogenic step is detrimental to the polarization, Meersmann *et al.* showed that krypton can be extracted efficiently using a single cycle piston pump.[19] Later, in another elegant solution, they proposed replacing nitrogen as the quenching gas during optical pumping by dihydrogen, which is then removed via catalytic combustion.[20]

^{3}He

Obviously, ^{3}He cannot be condensed easily using the cryogenic techniques previously described, due to its low boiling temperature. ^{3}He metastability exchange optical pumping (MEOP, more efficient than SEOP for this noble gas), on the other hand, uses pure ^{3}He , but at very low pressures (lower than 60 mbar) in order to get polarizations higher than 0.5.[21] The hyperpolarized ^{3}He produced therefore needs to be compressed in order to get a convenient volume. Two established techniques are typically used for this: i) peristaltic compressors (as in compact tabletop polarizers),[22, 23] and piston compressors.[24]

Special care has to be taken with relaxation of ^{3}He during its storage and transportation; magnetized boxes for housing polarized spins have been built in this purpose.[25] The boxes are magnetized either by permanent magnets or by electromagnets, and are designed to shield the gas from external stray fields. Permanent magnets are to be preferred for storage and transport purposes, *e.g.* when the gas has been polarized at an off-line facility. In an experimental situation, on the other hand, the flexibility of an electromagnet is appealing: it may allow tuning and/or rotation of the field, and it may allow openings in the box while still conserving the homogeneity of the field inside by adapting the current tracks appropriately.

3.1.2 Dissolution DNP

DNP occurs in vitreous samples containing radicals, which are excited by microwave irradiation, and the substrate to be polarized. In order to obtain the highest polarization, the sample has to be kept frozen at low temperature to ensure a polarization close to 1 for the electron spin. The sample is then transferred by sudden heating with a hot solvent, and rapidly retrieved from the polarizer. Obviously, to minimize relaxation the transfer time between dissolution and the NMR measurement has to be minimized, and, as for gaseous noble gases, the magnetic fields along the sample trajectory must be controlled to avoid regions of low magnetic field that would accelerate relaxation. For nuclei with short T_1, it is favorable to perform the DNP process and the NMR measurement in the same magnet (see below).

3.1.3 Transport and storage of parahydrogen

The transport and storage of parahydrogen is not a problem, as the conversion para ↔ ortho, i.e., from singlet to triplet state, can only occur through external dipolar relaxation. Thus parahydrogen can be transported and stored without too many precautions in a glass vessel, or even in a metal vessel if the walls are covered in Teflon. Due to the fast diffusion of the gas

(meaning that the gas atoms have frequent collisions with the walls), the quality of the latter coating is crucial for conservation of the para state.

3.2 The dissolution step

Several issues come with the dissolution step in aqueous media, which should be fast and as complete as possible: i) the potential formation of bubbles that destroy the homogeneity of the magnetic field, ii) strong interfacial tension that reduces the dissolution efficiency and may lead to aggregation, or at least segregation, of the hyperpolarized species (formation of gas hydrates for instance), iii) the risk of creating turbulent flow or transient convection,[26] and finally iv) the risk of sudden depolarization by relaxation.

These considerations have led to several different experimental setups being proposed, which differ in the magnetic field used, the dissolution scheme, the methods used to prolong hyperpolarization, and the systems synchronizing the introduction of the hyperpolarized species in the sample of interest with the triggering of the NMR sequence.

4 Instrumentation

4.1 Magnetic fields for maintaining and transferring polarization

4.1.1 Transport of hyperpolarized noble gases

As previously explained, transport from the production site (the optical pumping cell) to the spectrometer/imager requires the constant presence of a static magnetic field if polarization losses are to be minimized. Some simple solutions exist, such as the use of a mobile device in which frozen xenon is immersed in a bath of liquid nitrogen and subjected to a magnetic field delivered by a solenoid powered by car batteries (see Figure 2).

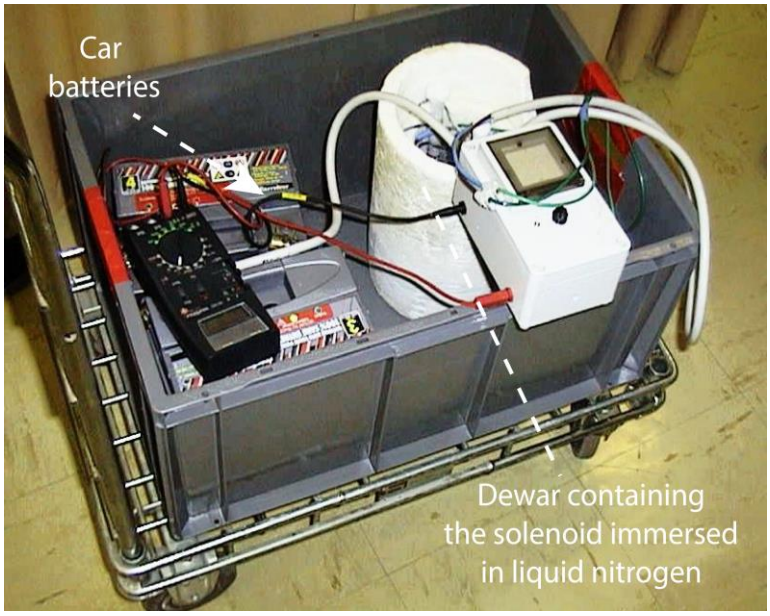


Figure 2: Picture of a chariot used at CEA Saclay for the transport of frozen laser-polarized xenon in a Dewar vessel, surrounded by a solenoid powered by car batteries. The Dewar is filled with liquid nitrogen.

Another elegant solution is to minimize the distance between the production site of hyperpolarized xenon and the NMR or MRI detection. This may involve i) development of transportable systems and/or ii) miniaturization of the optical pumping setup. In the latter case, the ultimate development was performed by Jimenez-Martinez *et al.*,[27] who proposed a microfabricated chip for optically polarizing ^{129}Xe. Such a device could be located in the fringe field of an NMR/MRI magnet. In the former case, several transportable SEOP systems have appeared in the literature.[28, 29, 30]

4.1.2 Magnetic tunnels and transfer lines for DNP

In dissolution-DNP, nuclear spins, hyperpolarized at cryogenic temperatures, need to be transferred to the NMR magnet for measurement, usually at room temperature. This is conventionally done by dissolving the hyperpolarized solid with hot solvent, before transfer to the NMR magnet. Transferring a hyperpolarized solution from a polarizer to a magnet, however, requires the solution to traverse regions of weak magnetic field, which may severely reduce the amount of hyperpolarization that reaches the NMR magnet. The passage of coupled spins through such a weak static field can also lead to the creation of long-lived states, that give rise to antiphase multiplets when transferred to high field for NMR detection.[31]

Therefore, in order to shield hyperpolarized solutions from relaxation mechanisms during the transfer between the polarizer and the NMR magnet, Bodenhausen *et al.* have designed a

modular ‘magnetic tunnel’ to interface the two units. The set-up is extensively described in ref. [29]. In short, it contains neodymium boron permanent magnets, held together by a 3D printed polymer structure, and positioned in four rows oriented such as to maximize the magnetic field strength in the center of the tunnel (B_{tunnel}>0.9 T). A hollow cylinder runs through the center of this structure to guide a 2.5 mm Teflon tube that carries the hyperpolarized fluid.

Any sudden change of the direction of the magnetic field may result in loss of magnetization. This is for example the case if the DNP polarizer and the NMR magnet have opposite static magnetic field directions, which requires an inversion of the spin polarization during the transport, or if the structure contains bends at the entrance or exit of the tunnel. The adiabaticity condition,

$$\frac{1}{B^2}\left|\vec{B} \times \frac{d\vec{B}}{dt}\right| \ll \gamma B$$

where $B=B_{stray}+B_{tunnel}$ is the total magnetic field, must be fulfilled at all times during transport. This was achieved by careful design of the tunnel so that the adiabatic ratio

$$A = \left|\vec{B} \times \frac{d\vec{B}}{dt}\right| / \gamma B^3$$

remained less than 1 throughout transport. Significant improvement factors have been observed for protons using this technology in dissolution-DNP experiments.

The transfer time between polarizer and NMR magnet can be several seconds, depending on the instrumental set-up, during which the hyperpolarization of nuclei may still decay severely despite the magnetic tunnel. Therefore, alternative strategies have been proposed. They consist in i) reducing the transfer time, and ii) transferring the hyperpolarized sample in the solid state - possibly at low temperature - as at low field the longitudinal relaxation time in solids at cryogenic temperatures is usually several orders of magnitude longer than in liquids for samples doped with radicals at elevated temperature.

For the purpose of reducing the transfer time, Kockenberger *et al.* have built a spectrometer based on a magnet with two isocentres.[32] The hyperpolarization is done in the upper compartment of the magnet, at a magnetic field of about 3.35 T and low sample temperature, while the lower compartment is at 9.4 T and room temperature for NMR measurement. The two parts of the magnet are very close (85 cm). Mechanical transfer of the hyperpolarized solid from the cryogenic region to the dissolution dock takes about 300 ms. An additional 700 ms is required to dissolve and transfer the solute to the NMR probehead. The transfer of the hyperpolarized sample is done in the solid state at cryogenic temperature, and the dissolution

step is performed at a magnetic field strength of *ca.* 5.5 T, which limits the loss of spin polarization due to T_1 relaxation. The liquid state enhancement factor obtained for [1-^{13}C] acetate were comparable to those reported for other ^{13}C - labelled compounds with long T_1 time constants using two separate magnets and pneumatic shuttling.

Recently, Meier *et al.* proposed the 'Bullet-DNP' method.[33] It consists in ejecting a bullet containing the frozen, hyperpolarized sample with pressurized helium gas, shooting it into a receiving structure in the NMR magnet, where the bullet is retained and the polarized solid is rapidly dissolved (Figure 3). The transfer is very fast, approximately 70 ms, and a magnetic tunnel along the entire transfer path limits polarization losses. The bullet itself is 12 mm tall, with an outer diameter of 3.9 mm, and has a 10 mm depth, 3.5 mm diameter concentric bore to accommodate the actual sample. A bullet can accommodate sample volumes of up to 80 µL. Using this technology, polarization levels around 30% have been obtained for 1-^{13}C pyruvic acid in solution. This is less than with state-of-the-art conventional d-DNP, for which up to 70% polarization has been obtained in solution; the authors ascribe the difference to lower polarization in the solid state (50%), and possible polarization losses during transfer and dissolution.

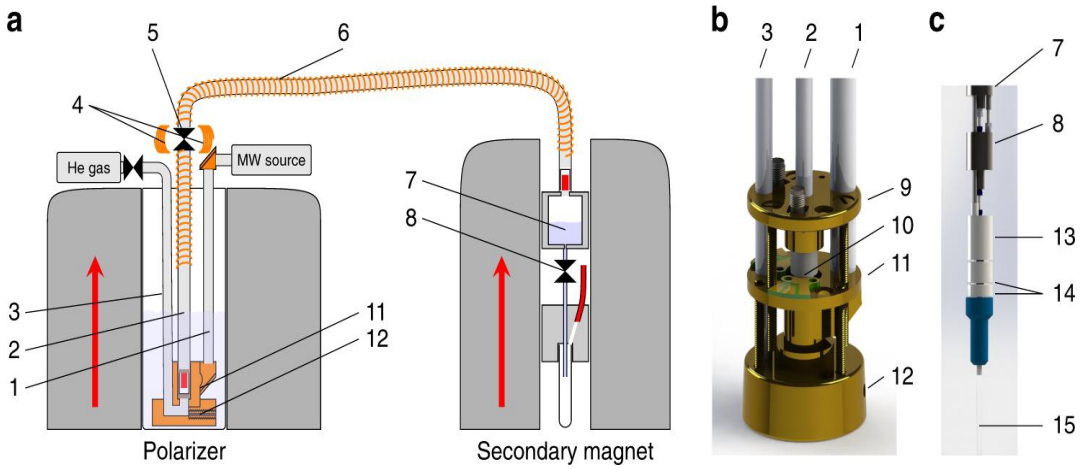


Figure 3: a) Sketch of the Bullet-DNP setup. b) Lower part of the DNP insert. c) Lower part of the injection device. (1): microwave tube; (2): sample tube; (3): drive gas tube; (4): Helmholtz coils; (5): valve; (6): transfer tube; (7): solvent reservoir; (8): pinch valve; (9), (11), (12): brass piece; (10): coil support; (13), (14), (15): 3D printed nylon pieces. Reprint from ref. [33].

4.1.3 Magnetic fields for hyperpolarization using parahydrogen

Dealing with direct hydrogenation techniques, it is well known that PASADENA (Parahydrogen and Synthesis Allows Dramatically Enhanced Nuclear Alignment) in which hydrogenation occurs at high magnetic field, gives different results from ALTADENA (Adiabatic Longitudinal Transport After Dissociation Engenders Net Alignment), in which the hydrogenation product is formed at essentially zero magnetic field and then adiabatically transported to high field for NMR acquisition. ALTADENA provides in-phase signals, while PASADENA gives antiphase signals.[34] In the SABRE (NMR Signal Amplification By Reversible Exchange) approach, spontaneous transfer also occurs at low field due to matching of the energy levels (the level anti-crossing (LAC) condition, as described by Ivanov *et al.*).[35, 36]

Let us consider the case of the SABRE method. After introduction of parahydrogen to the solution containing the iridium catalyst and the molecule of interest, the LAC between the hydride protons and the directly bound nitrogen atom of the target molecule occurs at low field (near 6 mT for the aromatic proton of pyridine for instance). This means that integration of a system for parahydrogen-based hyperpolarisation inside a high magnetic field is difficult, at least when homonuclear polarization transfer is targeted. The instrumentation for magnetic field cycling (from low field for the hyperpolarization step to high field for NMR detection) is very demanding, as it must be fast (faster than T_1 relaxation, unless singlet spin states can be created) and it must provide reproducible results. In the case of SABRE, several radiofrequency-driven methods have been proposed that enable direct polarization transfer at high magnetic fields from the hydride protons to the ^{15}N nuclei bound to the catalyst.[37, 38, 39] However spin-polarizing a heteroatom not directly bound to the catalyst is less straightforward; it is difficult for instance to imagine polarizing the ^{13}C nuclei of a substrate at high field. Nevertheless, this did not prevent Bordonali *et al.* from proposing a microfluidic NMR platform integrating a polarizer based on SABRE.[40] The authors proposed to use hydride proton signals to quantitatively distinguish molecules bound to the substrate, owing to their distinctive chemical shifts (around -20 ppm).

4.2 Dissolution setups

4.2.1 Hollow fiber membranes

The hydrophobic character of noble gases and hydrogen leads to unavoidable formation of bubbles and foams when trying to dissolve them in aqueous solutions such as biological media,

causing severe loss in spectral resolution due to the strong local gradients caused by variations in magnetic susceptibility. To circumvent this problem, the use of hollow fiber membranes, initially developed for blood oxygenation, is of great interest and has been shown to be efficient both for hyperpolarized ^{129}Xe [41, 42, 43] and for parahydrogen.[44, 45] In these membranes, the dissolution process is rapid and does not lead to significant depolarization. The gas/liquid surface is greatly increased while kept stationary. To maintain these conditions, however, the pressure gradient at this gas/liquid interface must be kept low to avoid liquid ingress into the membrane material or bubbling.[43] Such a gas-exchange module has also been used to infuse ^{129}Xe continuously into the arterial blood of live rats, using an extracorporeal circuit.[46, 47]

4.2.2 Gas-driven injection

Another strategy consists in forcing the hyperpolarized gas across a large surface area of the solution of interest.[48] Using this principle, 3D-printed NMR inserts have been conceived for controlled dissolution of hyperpolarized xenon produced in batch mode into a small solution volume, allowing detection with high sensitivity. A programmable syringe pump interfaced with the NMR console pushes nitrogen gas at a chosen flow rate that in turn pushes xenon contained in a reservoir placed on top of the NMR magnet (Figure 4). A mini bubble-pump is thereby constituted: the gas bubbles exiting from the pipe induce circulation of the solution into the closed-loop circuit, and in the lower part of this circuit NMR detection is performed using a micro-solenoid.

This device has been characterized in two different ways.

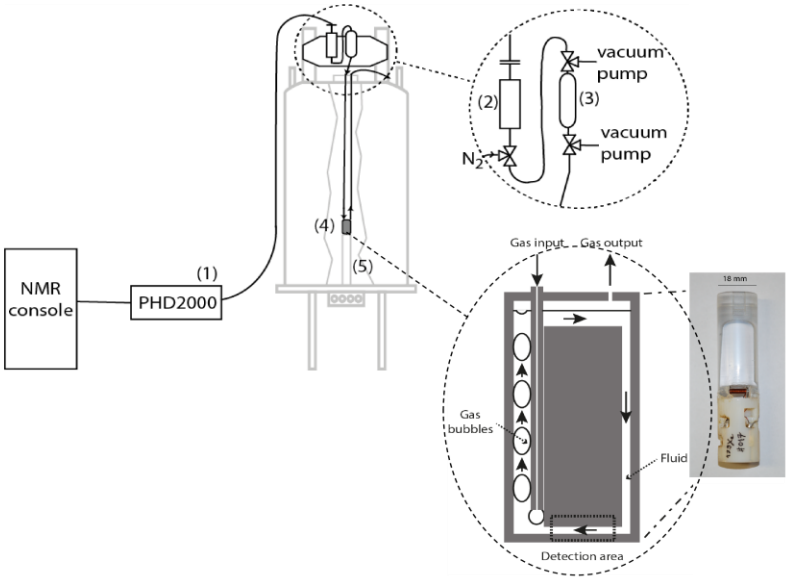


Figure 4: Principle of the bubble pump and global scheme of the setup. (1) Console of the syringe pump; (2) Syringe with buffer gas; (3) Reservoir with polarized xenon; (4) NMR cell containing the solution; (5) NMR probehead. Adapted from ref. [48].

Firstly, by using a molecular host with a known binding constant with the noble gas and with known concentration, it has been proved to be efficient in dissolving a large proportion of hyperpolarized xenon (estimated at 15%) in a controlled way. Note that this set-up could be combined with the use of hollow fiber membranes that could be inserted in the closed-loop circuit, to further facilitate dissolution of hyperpolarized xenon. Secondly, NMR velocimetry experiments have enabled the solution flow (in the micro-solenoid) to be linked to the gas flow. Asymptotic behaviour is encountered (Figure 5): at high gas flow rate the system saturates.

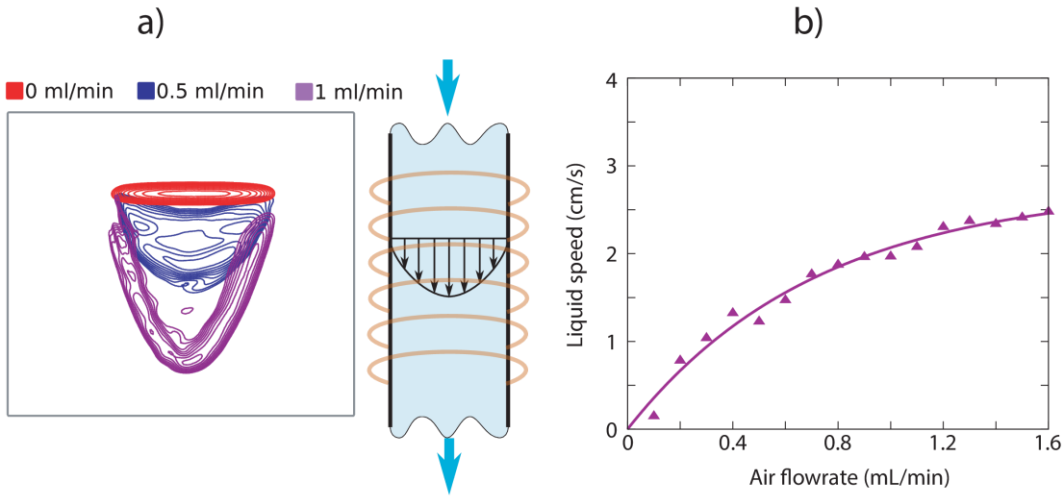


Figure 5: ^{1}H NMR velocimetry experiment performed to characterize the NMR cells previously described. a) Solution flow profiles at different gas flowrates; b) Liquid flow rate as a function of the solution flow rate. Adapted with permission from ref. [49].

The occurrence of jerky flow has been corrected by the use of a stopped-flow system. Such a disposable device exists in two versions:

- The micro-solenoid is plugged into the base of a commercial micro-imaging probe, such as a Bruker micro-5 probe, in place of the usual imaging coil.[48, 49] Such a setup allows both spectroscopic and imaging experiments with a single setting, as tuning and matching are performed using the variable capacitors of the commercial probehead. In this version, all nuclei can be studied (even those which resonate above ^{31}P, the upper limit of most commercial broadband probeheads, as for instance for the thallium isotopes ^{203}Tl and ^{205}Tl).
- The micro-solenoid is inductively coupled to the rf coil of a commercial probehead.[50] This system will now be described.

The inductively-coupled device (dubbed *WIFI-NMRS*) takes the form of an NMR tube, held in a spinner, with a a vertical rod extending to the top of the NMR magnet (see Figure 6) to allow injection of gas and reactants and to allow the angle between the microcoil of the device and the coil of the commercial probehead to be optimised. The gas inlet and the principle of the bubble pump previously described are retained.

Such a setup has several advantages with respect to plugging the micro-solenoid into the base of an imaging probe. First, it can work with all liquid state NMR probes. Second, the capabilities of the host probehead are maintained. For instance, proton decoupling can be used *via* the corresponding channel on the commercial probehead. In addition to allowing efficient dissolution and detection of hyperpolarized noble gases, these setups, whether electrically or inductively coupled to the parent commercial probe, can facilitate the study of slowly-relaxing nuclei (see refs. [49, 50]). The flow of the polarized solution through the closed-loop circuit, of which only a small region is used for NMR measurements, means that it is not necessary to leave an interscan delay, as the polarized sample is continuously replenished.

This is illustrated for a sample containing ^{13}C urea and U-^{13}C glucose (at a concentration ratio 0.4:1) in D_2O in a 5-mm *WIFI-NMRS* insert placed inside a 700 MHz BRUKER TCI cryoprobe. No hyperpolarization was used. Figure 7 shows the results obtained. In a) a ^{13}C spectrum was recorded in static mode (no solution flow) with the *WIFI-NMRS* insert, without optimization of the inductive rf coupling. In b) adjustment of the angle between the microcoil and the ^{13}C coil of the cryoprobe gave a sensitivity gain. However it can be observed (see Table 1) that the relative signal areas are not those expected. In particular the carbonyl signal of urea (at 165 ppm) – with a longitudinal relaxation time $T_1(^{13}C)$ = 39 s - is far lower than expected. When the solution was set in motion, Figure 7c, the quantitative character of the

spectrum was retrieved, illustrating an advantage of the flow approach with the sample staying in the high field region. Figure 7d, which shows the ^{13}C spectrum obtained under the same experimental conditions in the classical way, *i e.* in a 5-mm tube, also shows that the mass sensitivity provided by the *WIFI-NMRS* insert is very favourable. While the detection volume in the classical experiment is ca. 100 times that of the *WIFI-NMRS* micro-coil, the ^{13}C signal of urea is only multiplied by 2. Also, the ratio between the urea signal intensity and the other ^{13}C signals evidences the lack of quantitativity of the classical approach. Quantitativity is only retrieved when using the *WIFI-NMRS* insert with flowing solution.

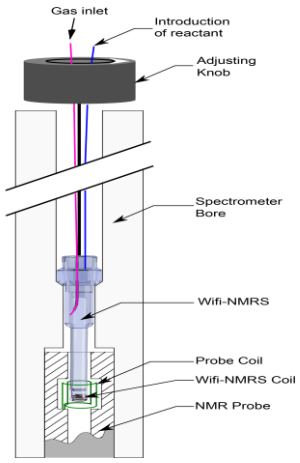


Figure 6: Principle of the *WIFI-NMRS* system.

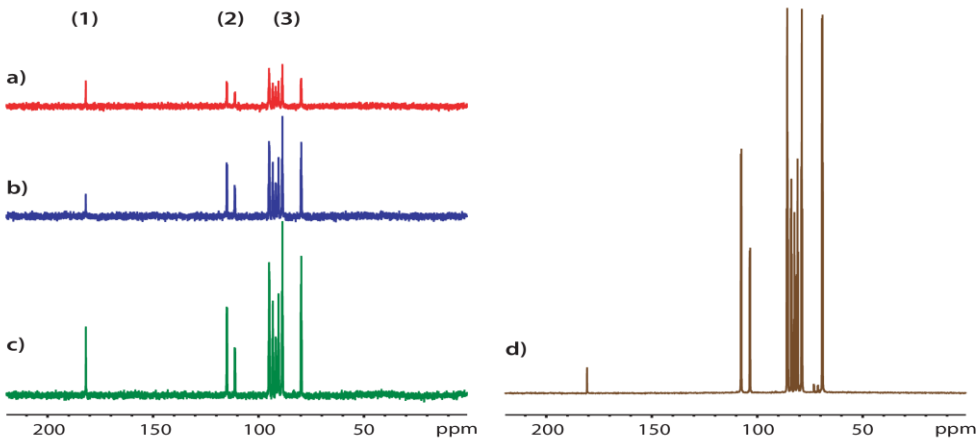


Figure 7: ^{13}C NMR spectra of a mixture of ^{13}C urea and U-^{13}C glucose at a concentration ratio of 0.4:1 recorded on a 16.4 T spectrometer equipped with a TCI cryoprobe. a) to c): spectra recorded with the *WIFI-NMRS* insert; a) in static mode, with a poor coupling between the microcoil and the coil of the cryoprobe; b) in static mode, after optimization of this coupling; c) in flow mode (activation of the bubble pump) with optimized rf coupling. d) spectrum recorded in a 5-mm tube under the same experimental conditions as for a)-c): 16 scans, interscan delay = 1 s.

		Ratio of integrals	
Signal(s)	Expected	Static	On-flow
(1)	0.40	0.16	0.39
(2)	1.00	1.11	1.08
(3)	6.00	6.00	6.00

Table 1: Normalized integrals of the ^{13}C signals in the spectra of Figure 7. (1) ^{13}C -urea signal; (2) signals of the anomeric carbons of glucose; (3) signals of carbons C_2 to C_6 of glucose. Static: spectrum of Figure 7b ; On-flow: spectrum of Figure 7c.

4.3 Trapping of species that accelerate nuclear relaxation

An important part of the developments deals with the separation of the freshly hyperpolarized species from species that enhance relaxation: traces of alkali metal for SEOP, radicals for DNP, hydrogenation catalysts for parahydrogen.

4.3.1 For laser-polarized species

Trapping is not a problem for noble gases polarized via SEOP, even when a spin-exchange optical pumping method employing an alkali metal such as rubidium is used. Given the low vapor pressure of these alkali metals (0.013 Pa at 360 K for Rb), a simple cold trap - for instance using an appropriate mixture of methanol and liquid nitrogen - is sufficient to remove them. It should also be noted that using MEOP to polarize ^3He, in addition to providing the best

quantum yield (the smallest number of photons required to polarize each atom) among the optical pumping methods, does not use any paramagnetic material.

4.3.2 For substances hyperpolarized by PHIP or SABRE

The PHIP and SABRE hyperpolarization processes occurr in non-aqueous solvents. Several different solutions have been proposed to the problem of transferring a hyperpolarized species to the aqueous phase without transferring any of the catalyst, which is typically toxic and therefore incompatible with biological applications. They include the use of molecules containing a side arm that can be hydrogenated, of heterogeneous catalysis, of metal-free catalysts, and of rapid phase transfer.

Side arm hydrogenation strategy

In the PHIP-SAH approach, Cavallari *et al.* incorporated a propargylic alcohol side arm on pyruvid acid. It is hydrogenated with para-hydrogen, then polarization is transferred to the ^{13}C carboxylate signal. The arm is subsequently cleaved, producing hyperpolarized [1-^{13}C]pyruvate directly usable for preclinical applications (Figure 8).[51]

Heterogeneous catalysis

Another way to facilitate separating the hyperpolarized species from the catalyst is to support the catalyst on a solid.[52] For instance, SABRE Ir-based catalysts have been successfully immobilized on various amino-functionalized particles: polymer microbeads,[53] TiO_2 /polymer nanoparticles with core-shell or 'comb' morphologies,[54] and silica particles,[55] without altering the signal enhancements.

Metal-free catalysts

In the classical SABRE approach, the activation of parahydrogen is performed using iridium-based hydrogenation catalysts. The presence of the toxic metal catalyst in solution shortens the hyperpolarization lifetime, and makes it difficult to produce pure hyperpolarized substances, for instance for biomolecular studies. Zhivonitko *et al.* proposed - both for PHIP and SABRE - to replace the metal-containing hydrogenation catalysts by molecular tweezers consisting of unimolecular frustated Lewis pairs (FLPs) containing functional centers connected by a chelating molecular link.[56, 57] Using some ansa-aminoborane derivatives they were able to obtain spontaneous ^{15}N hyperpolarization.[57]

Phase transfer

In the CASH-SABRE approach, Iali *et al.* showed that adding salt to the aqueous compartment of a biphasic solution accelerated the passage of the species of interest to the aqueous phase while keeping most of its hyperpolarization.[58] Barskiy *et al.* combined fast extraction of the hyperpolarized substance from the organic phase to the aqueous phase with rapid catalyst capture by metal-scavenging agents of the mercaptoalkyl-silica type.[59]

4.3.3 For dissolution-DNP hyperpolarization

The presence of a paramagnetic species, such as dissolved oxygen or polarizing agents, leads to a strong increase in the longitudinal nuclear relaxation rate. As shown by Miéville and co-workers,[60] one approach to removing paramagnetic N-oxide radicals, *e.g.* TEMPOL, from a solution is to reduce them to diamagnetic speies, *e.g.* H-TEMPOL, using a scavenger like sodium ascorbate (vitamin C). During the reduction process, ascorbate is transformed into ascorbyl radicals, which quickly disproportionate into ascorbate and diamagnetic 5-(1,2-dihydroxyethyl)furan-2,3,4(5H)-trione. Providing a solution free of paramagnetic species, the scavenging of TEMPOL by sodium ascorbate led to an extension of the proton longitudinal relaxation time by a factor up to 3 in acrylic acid. Similarly, the $T_1(^{13}C)$ of 1-^{13}C -acetate was significantly extended.

Counter-intuitively, adding trace amounts of paramagnetic agents such as gadolinium chelates to DNP samples containing trityl radicals has been shown to substantially improve ^{13}C hyperpolarization.[61, 62, 63] The principle lies in the lowering of the trityl electron Zeeman relaxation time by the lanthanide ion, with no significant effect on the relaxation times (T_1, T_2) of the nuclei. The addition of Gd^{3+} chelates has, however, less advantages for the DNP efficiency at higher magnetic fields.

One solution to overcome the limitation posed by the use of stable radicals such as trityls, BDPA (1,3-bisdiphenylene-2-phenylallyl), and nitroxides, that shorten the T_1 of nuclei of interest, is to physically separate the free radicals from the hyperpolarized solutions.[64] The use of non-persistent UV-induced radicals (formed at 77 K by UV irradiation of frozen aliquots, disappearing above 170 K) has also been proposed.[65, 66] The first proof of concept using a non-persistent radical generated from pyruvic acid was limited to low ^{13}C polarization compared to trityl radicals, which was attributed to the broad EPR spectrum of the pyruvic acid radicals. As the presence of pyruvic acid can interfere with cell metabolism, and as some

substrates are photo-sensitive and can degrade during the UV irradiation, recent work has focused on non-persistent radicals generated with visible light. [67]

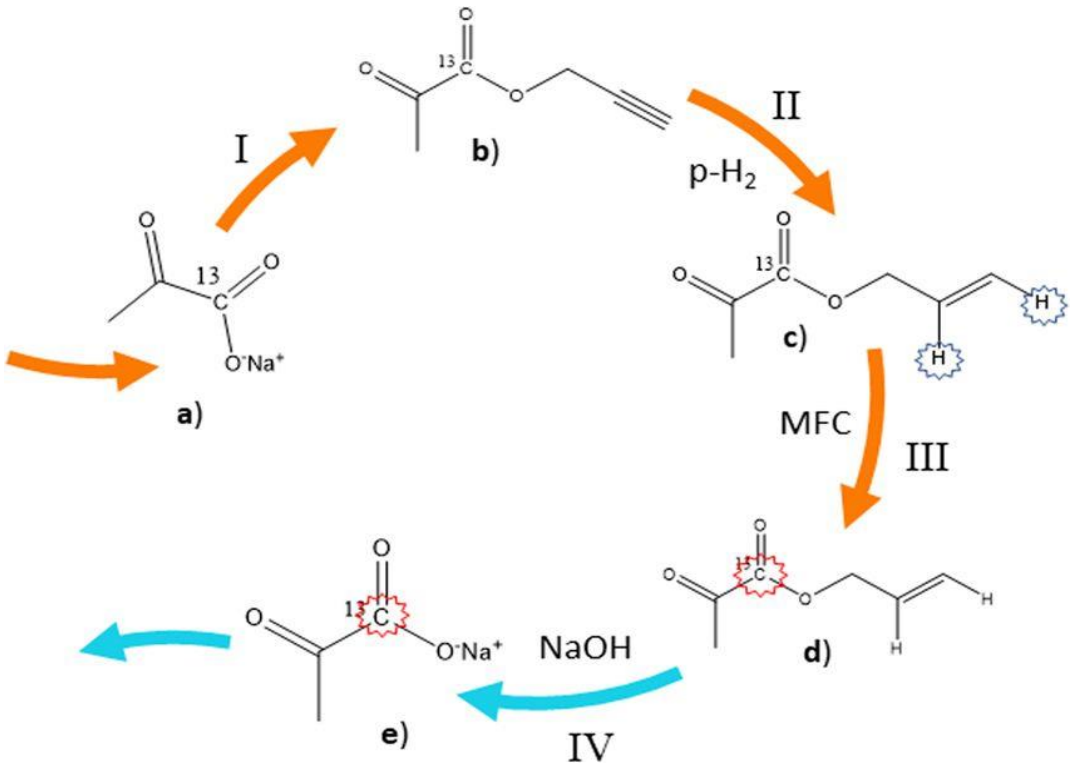


Figure 8: Schematic representation of the PHIP-SAH procedure, going from functionalization of [1-^{13}C]pyruvate (I) to hydrogenation of the triple bond (II), polarization transfer to the ^{13}C carboxylate signal (III), to ester hydrolysis (IV). Reprinted from ref. [51].

4.4 Triggering systems

Since the nuclear spin populations of hyperpolarized species are not in equilibrium, the main condition that must be met to optimize their use is to minimize the time between sample injection and NMR measurement. The practicalities are similar to those of real-time monitoring of chemical reactions via NMR. An example of a triggered system for continuous NMR monitoring of a synthesis in an industrial environment is given in ref. [68].

A minima the NMR pulse sequence should be triggered by sample injection. Bowen and Hilty [69] used for this purpose a contactless conductivity detector, with wide applicability to a variety of polar and non-polar solvents. Other detectors, based on optical methods, have also been proposed.[70] Most of the time, such monitoring devices are associated with

microfluidics and micro-sized NMR detection, which are beyond the scope of this article but have been widely reviewed, for instance in ref. [71].

5 Methods

The transient character of hyperpolarization, and the difficulty of keeping the concentrations of hyperpolarized species constant over time, mean that classical 1D- or nD-NMR pulse sequences are not appropriate. It is also important that the pulse sequence preserve most of the polarization: the use of a 90° flip angle pulse implies a total loss of polarization in the active sample volume after excitation. Also, if the polarization is high, inversion of spin populations can be difficult due to radiation damping [72] and/or maser effects.[73, 74]

Thus, in addition to the use of small flip angle excitation pulses, various strategies can be employed to make best use of the available hyperpolarization.

- In the case of chemical exchange, using frequency-selective excitation to preserve the main reservoir of hyperpolarization.
- Using so-called ultrafast sequences. Their common feature is that they use pulsed field gradients to perform spatial encoding and to enable different regions of the sample to experience different rf excitations and delays.
- Permanently renewing the reservoir of hyperpolarization and coupling it to adapted pulse sequences.
- Transferring the hyperpolarization to nuclei with long T_1 or to singlet spin states.

Let us describe the first two strategies.

5.1 Sequences using frequency-selective pulses

These sequences work in the case of chemical exchange between different hyperpolarized reservoirs. The strategy here is to avoid perturbing the main hyperpolarization reservoir by radiofrequency irradiation, focusing instead on a spectral region of interest. The exchange dynamics of the system then ensure replenishment of the polarization of the species of interest. This represents a direct detection method, as opposed to the indirect method provided by the CEST approach (see below).

Examples of such situations can be found in the domain of ^{129}Xe NMR-based biosensors, succinctly presented in Section 2. Fast repetition of the sequence [*soft excitation - detection*] in which the soft pulse selectively excites the region of the spectrum corresponding to the caged

xenon environment, at a rate close to that of the in/out xenon exchange, makes it possible to achieve a low detection threshold for the biosensors.[75] In the same vein, in the SABRE approach, frequency-selective pulses applied to the hydride signals reveal polarization transfer from the axial ligand on the catalyst to the substrate.[36]. Also, soft pulses on the hydride signals and protons of the substrate can be used to transfer polarization from the former to the latter at high magnetic field.[76]

5.2 Ultrafast sequences

The structure of a classical nD NMR experiment, that relies on having a reproducible magnetization before the initial excitation pulse, is definitely not appropriate for most hyperpolarization setups, which lack reproducibility in the concentration and/or polarization of the hyperpolarized species. Ultrafast methods have been developed to acquire in a single shot all the information normally acquired in an extended 2D experiment. The excitation part of spatial encoding (SPEN) pulse sequences is based on the principle of dividing the sample into multiple slices by the combined use of frequency-selective or chirped excitation pulses and pulsed field gradients, just as in slice selection in MRI.[77] Detection (decoding) is carried out via an Echo Planar Imaging (EPI) process. The loss of sensitivity linked to the sample slicing is compensated for by the hyperpolarization. These sequences are extensively described in ref. [78]; we will only describe here some of those developed for correlation and self-diffusion NMR, and one applied to the case of exchange, for instance in ^{129}Xe NMR.

5.2.1 SPEN sequences

In a pioneering work, Frydman *et al.* employed an ultrafast scheme to analyze compounds at low concentration, pushing the limit by performing ^{15}N-HSQC on ^{15}N-enriched pyridine, hyperpolarized by DNP at submicromolar concentrations, within *ca.* 0.1 s.[79] This experiment was then adapted to other substances hyperpolarized by dissolution DNP [80] or by SABRE [81, 82] for developing various scalar correlation sequences, and enabled fast analysis of compounds or mixtures of compounds at low concentrations.

Such approaches are also of interest for self-diffusion measurements on hyperpolarized substances.[83, 84] However, spatial encoding along the NMR tube may lead to sources of bias such as convection along the principal axis of the tube (leading to displacement of spins between the encoding and acquisition steps) that must be taken into account and corrected. In another application of this concept, Ahola *et al.* introduced an ultrafast diffusion-relaxation

correlation experiment based on multidimensional Laplace NMR.[85] They showed reductions of orders of magnitude in the experimental time needed for analysis of complex mixtures.

5.2.2 Ultrafast Z-spectroscopy

Z-spectroscopy is an NMR approach widely used to detect metabolites at low concentration when they are in exchange with a large pool of magnetization, for example the amine protons of amino acids exchanging with water (glutamic acid is often chosen as a model). The exchange must be slower than the frequency difference between the two magnetic environments, so that their signals are resolved. The approach used in this family of experiments is known as *CEST*, or *Chemical Exchange Saturation Transfer*. It consists in saturating, usually *via* CW rf irradiation, the frequency of the small reservoir signal (*e.g.* the amine proton of glutamic acid) and detecting the effect on the amplitude of the main signal (water) and observing the depletion of the large reservoir signal due to the exchange. Compared to the direct detection method, in which fast succession of the sequence {frequency-selective excitation at the small reservoir frequency - detection} could also take advantage of the exchange, CEST further benefits from reduced accumulated noise as the number of acquisitions is reduced. This is well documented.[86, 87]

When the frequency of the small reservoir signal is unknown, a classical technique is to sweep the saturation frequency in discrete steps and for each value to record the change in the main signal. Because it monitors the change in Z magnetization of the large pool as a function of the saturation frequency, this is called Z-spectroscopy. Imagine now performing this experiment with a hyperpolarized species: the case of ^{129}Xe NMR-based biosensing for instance, where xenon caged in a host molecular system at low concentration is in exchange with xenon in the bulk. Here, the NMR experiment that was proposed by Schröder *et al.* in 2006 to boost detection sensitivity, is called HyperCEST.[88] This experiment has been shown to be more efficient than direct detection with frequency-selective pulses, but measuring a Z-spectrum is difficult because hyperpolarized xenon magnetization varies between scans.

We tested such an experiment some years ago with a cryptophane derivative bearing a nitrilotriacetic function designed to chelate various metal cations. We found that for some cations tested, such as Cd^{2+}, Zn^{2+} and Pb^{2+}, the resonance frequency of caged xenon took a characteristic value.[89] In a sample containing Pb^{2+} ions at micromolecular concentration, a ^{129}Xe Z-spectrum was recorded in order to separate the responses of free cryptophane molecules from those chelating lead cations (see Figure 9). Such an experiment was tedious,

as for each saturated frequency value an image had to be recorded as a reference to correct for the effects of the magnetization fluctuations.

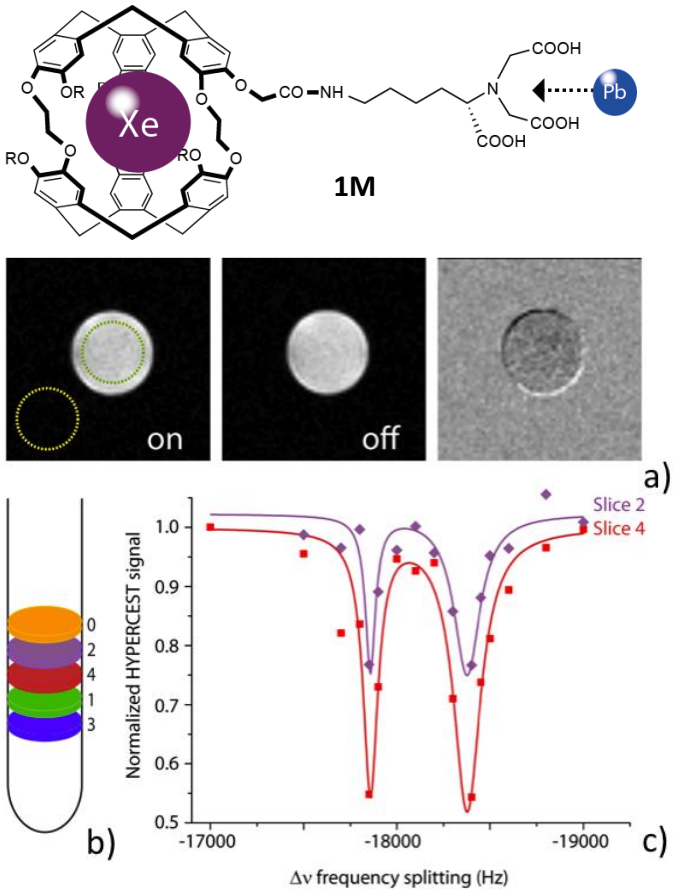


Figure 9: Detection of lead cations *via* ^{129}Xe NMR using a dedicated xenon host molecule **1M**. (a) HyperCEST-EPI axial images of a lead-containing sample. Left image: saturation at the Xe@**1M**-Pb^{2+} frequency. Middle image: off-resonance saturation. Right image: 'on-off' difference. (b) Axial slices recorded for each point of the Z-spectra. (c) Z-spectra recorded by integration of the images with different offsets. Adapted with permission from ref. [89].

In 2013, Jerschow *et al.* proposed an alternative for ^{1}H NMR, ultrafast Z spectroscopy (UFZ), using a pulse sequence in which the saturation step is performed in the presence of a gradient pulse.[90] Such a scheme saturates each frequency in a different slice of the NMR tube. After the readout pulse, detection is performed in the presence of another gradient, which gives the profile of the NMR tube with the saturated region(s). In order to get rid of the sample profile,

a second scan may be performed without saturation; the difference between these two scans directly reveals the signals of the nuclei interacting with those of the main reservoir.

This sequence has also been applied to ^{129}Xe NMR-based biosensing (Figure 10), showing its utility in the case of hyperpolarized species. Even where the hyperpolarized xenon magnetization fluctuates with time, the Z-spectrum is not seriously affected as it is obtained in only two scans.[91, 92] To increase the signal-to-noise ratio (SNR), averaging can now be performed on a spectrum-by-spectrum basis. The other advantage of using this approach for hyperpolarized species lies in its relative insensitivity to static field inhomogeneities (lines are still broadened by transverse static field gradients). Various derivatives of the basic sequence have been proposed:

- Acquiring multiple echoes by applying 180° pulses during acquisition enables one to increase the SNR (see Figure 10).
- Replacing the fixed pulsed field gradient during acquisition in the 1D sequence by a variable gradient gives rise to chemical shift CEST imaging, usually employed with radial sub-sampling to minimize relaxation effects.[93]

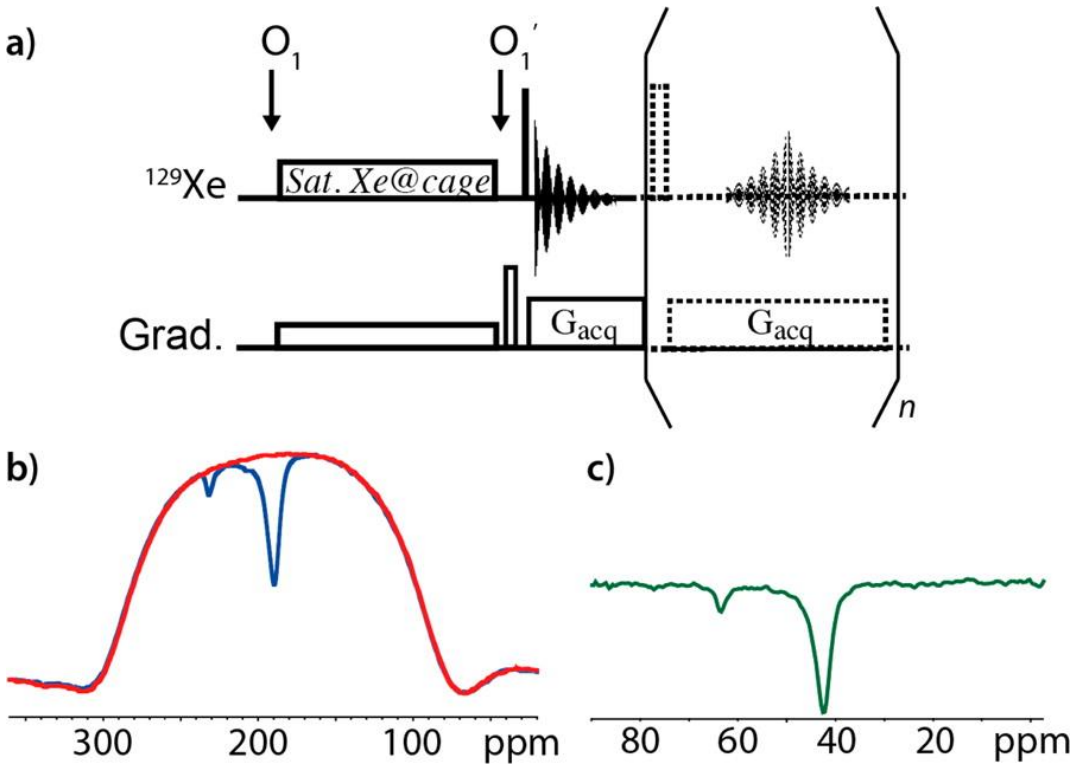


Figure 10: (a) Modified pulse sequence for UFZ spectroscopy. (b) ^{129}Xe UFZ spectrum of a mixture of cryptophanes in water recorded in one scan without (blue line) and with (red line) CW saturation. (c) Normalized difference between the blue and red spectra in (b). Reprinted with permission from ref.[91].

Note also that in SABRE , Knecht *et al.* have shown how to reveal intermediate states and the presence of a catalyst by the monitoring of hydride proton signals, using CEST from the ortho-H_2 signal.[94]

6 Three applications in biology

6.1 A noble gas study of biological cells

The study of biological cell suspensions with hyperpolarized species is particularly demanding:

- The fragile cells do not tolerate violent agitation that could damage them.
- Cells require to be kept in a suitable physiological environment. This aqueous medium (containing salts and relaxation agents) is often unfavorable to the preservation of the hyperpolarization of the species studied.
- Biological processes can take place over long periods (hours or even days). The observation system must therefore make it possible to maintain the cells under physiological conditions and to reintroduce the hyperpolarized species at different times.

Thus, any device for hyperpolarized measurements on cells must meet these criteria: i) it must be biocompatible, so as not to cause the degradation of the biological system studied; ii) the mixing between the hyperpolarized species and the solution containing the biological sample should be done as gently as possible, to avoid the effects of shearing that would degrade the cells, but the device must be as close as possible to the detection zone because of the increase in the rate of depolarization of the species once dissolved; and iii) it must keep biological parameters such as temperature and pH constant, and compensate for any evaporation of the medium over time.

6.1.1 3D-printing and biological material

As highlighted in Section 4.2.2, the availability of 3D-printing and its constant evolution facilitate the building of integrated devices employing hyperpolarized species in biological applications. However, 3D-printed devices have some drawbacks compared to polydimethylsiloxane (PDMS) structures obtained by conventional lithography. One of these is linked to the fact that stereolithography and inkjet 3D printing often use proprietary photopolymers that are toxic or largely incompatible with live biological matter.[95, 96] This cytotoxicity generally results from the release of unreacted monomers and/or photo-initiators.

To overcome these limitations, many research efforts have been directed towards formulation of biocompatible resins such as hydrogel matrices composed of polyethyleneglycol diacrylate derivatives [97] or acrylate modified biomolecules,[98] as well as towards improved photoinitiators.[99] Nevertheless, these lab-made resins can be only used with open source 3D printers and need to be fully characterized (chemical, mechanical and biological properties) before their use in microfluidics. While progress is encouraging, longer-term *in vitro* and *in vivo* studies remain to be performed.

6.1.2 ^{129}Xe NMR for the study of biological cells

It has been shown some years ago that the ^{129}Xe NMR spectrum of a suspension of living cells exhibits two signals, the main one corresponding to xenon in the medium, and the other, less shielded, to xenon inside cells.[100] The fact that the two environments are separated in the spectrum is very useful: i) for red blood cells, the splitting between the two signals indicates their oxygenation level (the shift of the inner signal being related to the amount of oxyhaemoglogin);[101] and ii) the exchange rate of xenon between the external medium and the inner compartment of the cell can be easily measured. The latter has been used to discriminate between cells that are sensitive to or resistant to chemotherapy.[102]

The 3D-printed devices presented in Section 4.2.2 have been tested for two cell types: yeasts (Saccharomyces Cerevisiae) and mammalian cells (A549). In the case of A549, a high mortality of the cells was observed after 30 minutes spent in the device: the cell density dropped from 300 million to 100 million per mL, and among the remaining cells, the viability measured with trypan blue was only 50% (Figure 11). The tests with yeasts also showed rapid degradation of the cells. In order to make the device biocompatible, a parylene layer was therefore deposited on the channel surface through chemical vapor deposition (CVD). The same measurements were performed in the presence of the two cell types. After 4 h of contact, the A549 cells had a 97% viability rate, with a stable cell density, and the yeasts showed normal growth (with OD_{600nm} increasing from 0.5 to 1.9 in 4 h), demonstrating the protective effect of parylene.

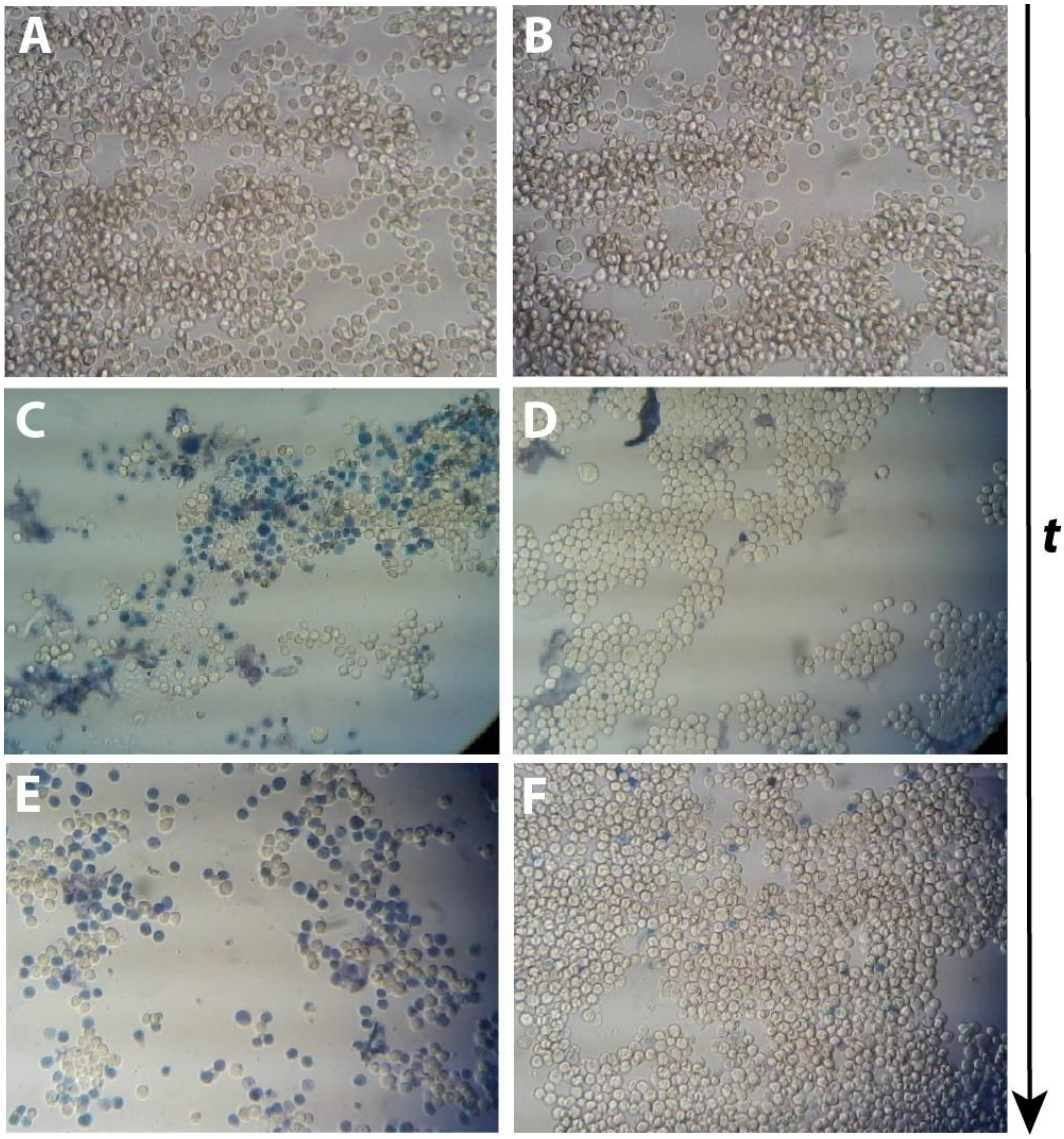


Figure 11: Trypan blue exclusion assays performed on A549 cells placed inside a 3D printed NMR micro-device. A, C, E: uncoated device; B, D, F: device coated with parylene N. Images recorded A, B: at the beginning of the experiment; C, D: after a residence time of 30 min; E, F: after 4 h. Dead cells appear in blue. Scale bar 100 µm.

The ability of the device to monitor, through hyperpolarized ^{129}Xe NMR, the effect of adding toxic substances to a biological cell sample was also tested. An 8 mm inductively-coupled *WIFI-NMRS* insert equipped with a ^{129}Xe -tuned microcoil was filled with 600 µL of a yeast suspension of OD_{600nm} = 20. Spectra were acquired every 0.5 s in order to follow the temporal evolution of the system. Laser-polarized xenon was injected with a flow rate of 1 mL min^{-1}. In parallel, a quick injection of 200 µL of a 40 mM solution of $CoCl_2$ was performed (Figure 12). While the less shielded ^{129}Xe signal, corresponding to the inner cell compartment was

unchanged, the more shielded ^{129}Xe signal from the bulk experienced a frequency shift due to the paramagnetic Co^{2+} cations. The fast spectral response shows the efficiency of the experimental setup.

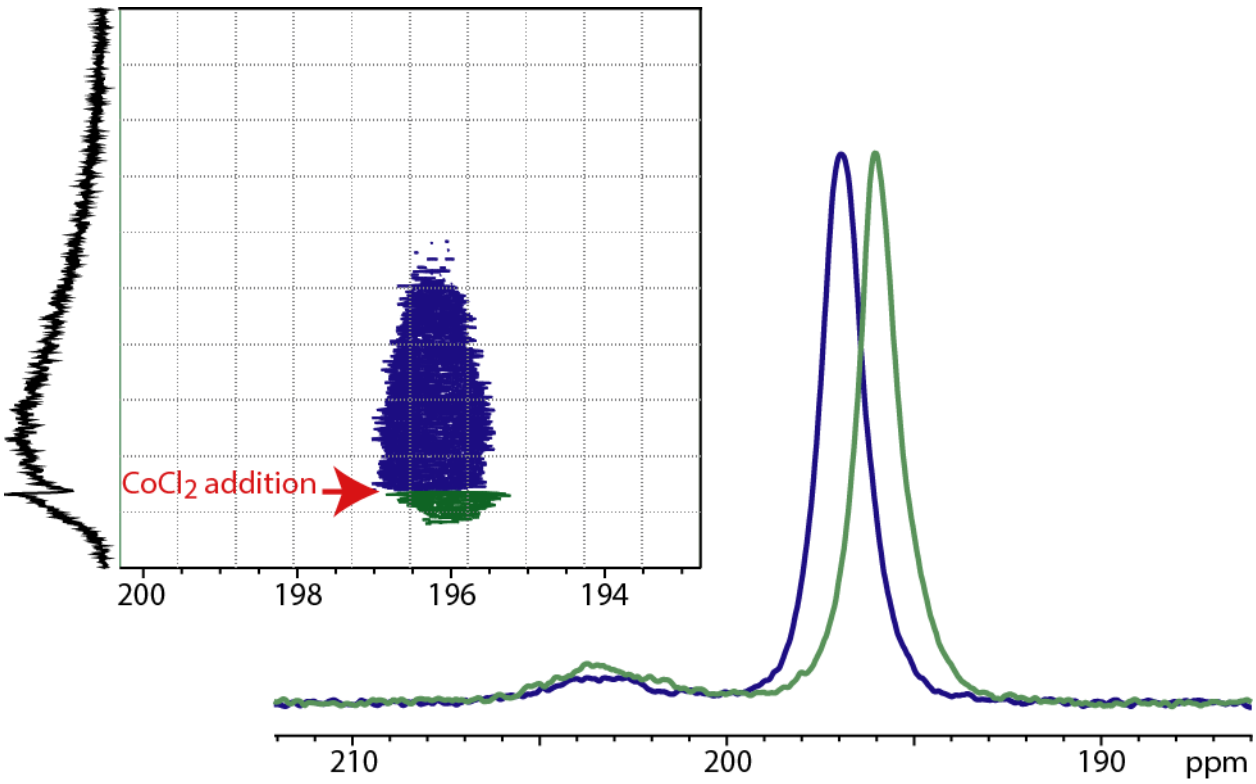


Figure 12: Monitoring through ^{129}Xe NMR of the introduction of a toxic substance, $CoCl_2$, to a yeast suspension. On the contour plot (frequency in abscissa, time in ordinate), the recording of each spectrum, recorded before (green) or after (blue) $CoCl_2$ addition, took 0.5 s.

6.2 Characterization of a enzymatic reaction *via* dissolution DNP

Beta-galactosidase is an enzyme that yses beta-galactosides into simple sugars and has been extensively studied. The substrate studied here was *o*-nitrophenyl β-D-[1-^{13}C; ^{2}H] galactopyranoside (Galp-onp).[103] The role of the ^{2}H-labeling was to limit the relaxation rates $R_1(^{13}C)$ of the quaternary carbon atoms. ^{13}C was hyperpolarized by dissolution DNP in DMSO in the presence of the trityl radical OX063, and then dissolved in Phosphate Buffer Saline (PBS) at pH 7.4 before being mixed with the enzyme 5 s later. The first point of the kinetic measurements started at 0.5 s after this last step. The ^{13}C NMR spectra obtained were

the result of two parallel phenomena: i) hydrolysis and transglycolization reactions due to the enzyme, and ii) ^{13}C depolarization over time.

Various reaction intermediates were thus identified. In addition to the intermediate *C* found at high concentration, already known in the literature, other intermediates *A*, *B* and *E* present at lower concentrations were also highlighted. In order to compensate for the decay of the hyperpolarized ^{13}C signal over time, the authors proposed a model taking into account this depolarization. The kinetics of transglycolysis and hydrolysis by beta-galactosidase thus understood are presented in Figure 13.

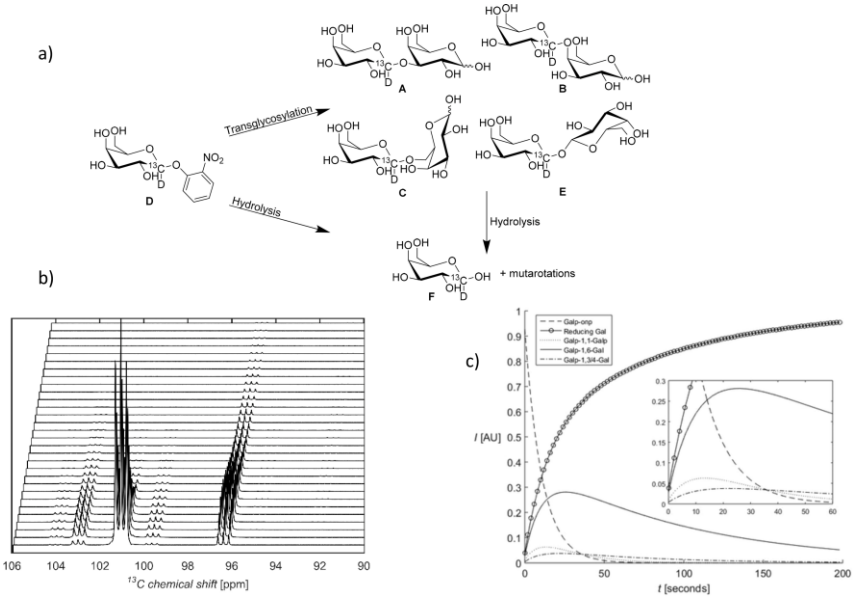


Figure 13: a) Global scheme for the transglycosylation and hydrolysis reaction of β-Galp-onp by β-galactosidase, as observed by ^{13}C NMR after hyperpolarization by dissolution DNP. b) Evolution of the ^{13}C NMR spectrum during the reaction. c) Curves for the evolution of the intensities of various ^{13}C signals, after compensation for depolarization. Reprinted with permission from ref. [103].

The high sensitivity and good temporal resolution of dissolution-DNP NMR prove here to make it a tool of choice, providing a better understanding of the mechanism of action of β-galactosidase by highlighting intermediates which could not have been observed by other methods because of their low and transient concentration.

6.3 Monitoring of the activity of an enzyme using parahydrogen-hyperpolarization

Fumarate is a metabolite important in the Krebs cycle. It is converted into malate by the enzyme fumarase in one step, a process that can be followed *in vivo* by ^{13}C NMR. While it is possible to produce hyperpolarized [1,4-$^{13}C_2$] fumarate via dissolution-DNP, a cheaper and faster way is to use PHIP, as shown by Eills *et al.*[104] The unsaturated precursor was [1–^{13}C] acetylene dicarboxylate, which in the presence of a ruthenium catalyst and parahydrogen, is transformed into hyperpolarized [1–^{13}*C*]fumarate. Figure 14 shows ^{13}C NMR monitoring of the enzymatic conversion of [1–^{13}C] fumarate into both [1–^{13}C]malate and [4–^{13}C]malate in a suspension of lysed cells.

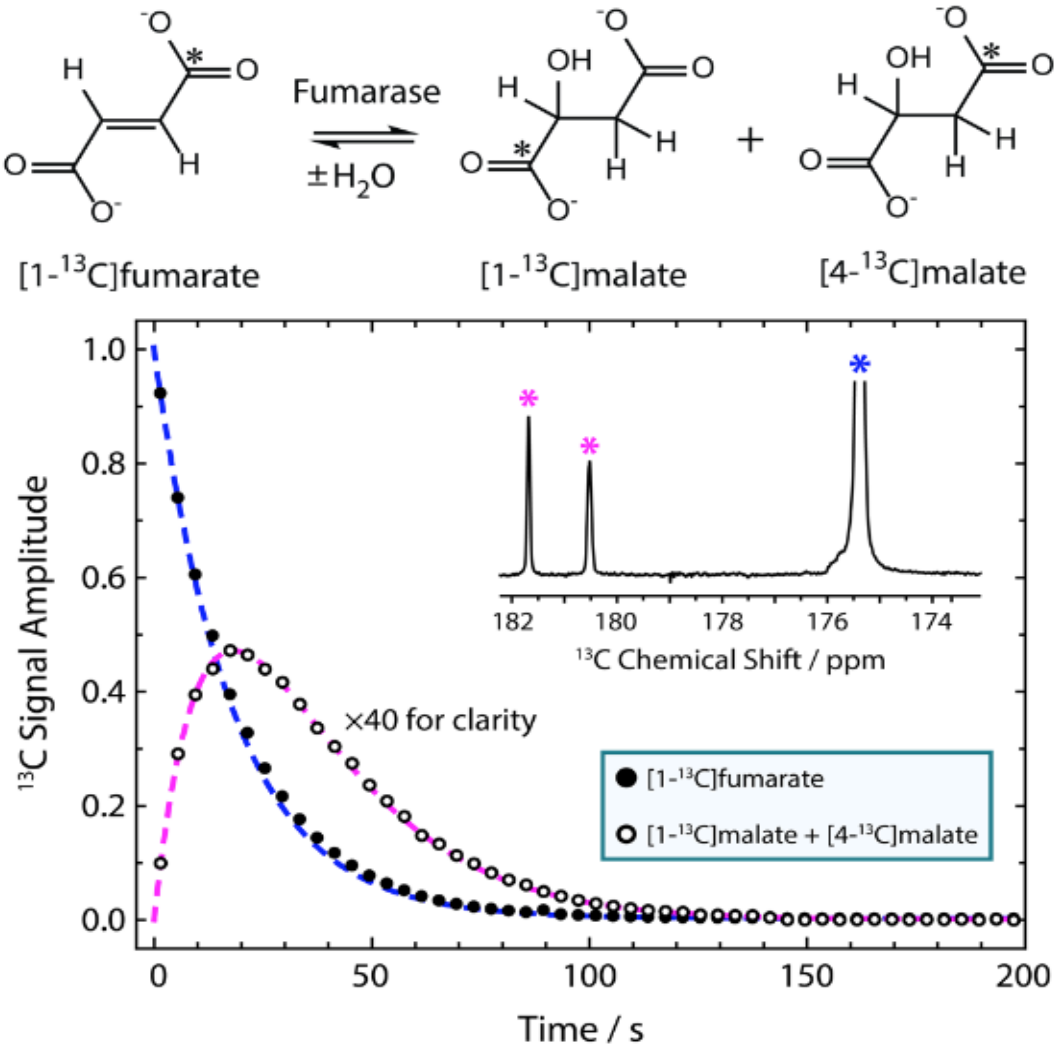


Figure 14: Monitoring through ^{13}C NMR of the metabolism in cell suspensions of [1–^{13}C] fumarate hyperpolarized *via* PHIP. Reprinted from ref. [104].

7 Concluding remarks

A number of integrated devices combining microfluidics, micro-detection and hyperpolarization have been described in in the literature. While a few use laser-polarized ^{129}Xe [105, 48] and CIDNP,[106] the majority of them deal with hyperpolarization *via* parahydrogen,[107, 108] the cheapest method, which is becoming more versatile. Recently, Bordonali *et al.*,[40] as already mentioned, proposed a device based on a micro-SABRE platform mounted on the core of a Bruker microimaging probe (a similar mounting was used for the device conceived by Causier *et al.*[48] for hyperpolarized ^{129}Xe NMR). Eills *et al.* conceived an integrated device that combines PHIP hyperpolarization with a high-sensitivity transmission-line micro-detector.[109] In their setup the hydrogenation reactor is integrated into the microfluidic chip itself, in order to reduce the polarization losses arising from T_1 relaxation.

Each of the three hyperpolarization methods presented here has its own advantages and preferred field of application.

Due to the responsiveness of xenon to its local environment, its solubility in various media, and its capacity to be encapsulated in cage molecules, it constitutes a powerful probe of biological processes. Reaching nuclear polarizations of more than 50% *via* optical pumping in a few minutes has become routine, and observing xenon, which has a gyromagnetic ratio close to that of ^{13}C, is easy. However, the problem is that transferring the polarization from ^{129}Xe to other nuclei is not efficient due to its gyromagnetic ratio, its large van der Waals radius, and the short residence time in complexes with other atoms or molecules. It condemns us to observe only this atom, which renders the monitoring of biological or chemical processes less straightforward.

Dissolution DNP is undoubtedly the most versatile method, as every nucleus with non-zero spin can in principle be hyperpolarized. However, it requires heavy and expensive equipment, which precludes its use in many laboratories. The time required to produce hyperpolarized species is also rather long, which limits dissolution DNP to a batch-mode approach.

Hyperpolarization from parahydrogen is undoubtedly the cheapest method. Its lack of versatility is starting to be overcome, *via* two different approaches: either the tethering of

unsaturated and cleavable groups onto the molecule of interest, or, in the case of the SABRE approach, intermolecular transfer of hyperpolarization through chemical exchange from amine groups bound to an iridium catalyst.[110]

While hyperpolarized xenon exhibits relaxation times compatible with *in vivo* experiments, most ^{13}C or ^{15}N T_1 values encountered *in vivo* are too short for safe metabolic profiling. However both DNP and parahydrogen hyperpolarization can benefit from direct production of singlet states,[111] for which depolarization times are significantly longer than the corresponding longitudinal relaxation times. For instance, [1,2-$^{13}C_2$] pyruvic acid hyperpolarized either via d-DNP [112, 113] or SABRE [114] directly produces singlet states that are less susceptible to depolarization.

This review has focused on the three most common hyperpolarization techniques, but several other methods are obviously also powerful or promising, including hyperpolarization from nitrogen vacancy (NV) centres in diamond.[115] In this last approach, hyperpolarization builds up over several minutes at room temperature and can provide high enhancement of the NMR signal.

Acknowledgments

The authors are indebted to Gaspard Huber (CEA) for a careful reading of the manuscript, and discussion. Support from the French Ministry of Research (project 17-LCV2-0002-01 LabCom DESIR) is acknowledged.

Abbreviations

ALTADENA: Adiabatic Longitudinal Transport After Dissociation Engenders Net Alignment
BDPA: 1,3-bisdiphenylene-2-phenylallyl
CASH-SABRE: Catalyst separated hyperpolarization through signal amplification by reversible exchange
CEST: Chemical Exchange Saturation Transfer
CIDNP: Chemically-Induced Dynamic Nuclear Polarization
CVD: Chemical Vapor Deposition
DMSO: Dimethylsulfoxide
DNP: Dynamic Nuclear Polarization
d-DNP: Dissolution DNP
EPI: Echo Planar Imaging
HSQC: Heteronuclear Single Quantum Coherence
LAC: Level Anti-Crossing
MEOP: Metastability Exchange Optical Pumping
NV: Nitrogen Vacancy
OP: Optical Pumping
PASADENA: Parahydrogen and Synthesis Allows Dramatically Enhanced Nuclear Alignment
PBS: Phosphate-Buffer Silane
PDMS: polydimethylsiloxane
PHIP: Para-Hydrogen Induced Polarization
PHIP-SAH: Para-Hydrogen Induced Polarization Side Arm Hydrogenation

SABRE: signal amplification by reversible exchange
SEOP: Spin Exchange Optical Pumping
SNR: Signal-to-Noise Ratio
SPEN: Spatial Encoding
SQUARE: Surface Quadrupolar Relaxation
WIFI-NMRS: Wireless Inductive coupling and Flow for Increased NMR Sensitivity

References

[1] E. Wilhelm, R. Battino, R. J. Wilcock, Low-pressure solubility of gases in liquid water, Chemical Reviews 77 (2) (1977) 219–262.

[2] M. H. Levitt, Singlet and Other States with Extended Lifetimes, in: R. K. Harris (Ed.), Encyclopedia of Magnetic Resonance, John Wiley & Sons, Ltd, Chichester, UK, 2010.

[3] G. Huber, L. Beguin, H. Desvaux, T. Brotin, H. A. Fogarty, J.-P. Dutasta, P. Berthault, Cryptophane-Xenon Complexes in Organic Solvents Observed through NMR Spectroscopy, The Journal of Physical Chemistry A 112 (45) (2008) 11363–11372.

[4] M. Kunth, C. Witte, L. Schröder, Quantitative chemical exchange saturation transfer with hyperpolarized nuclei (qHyper-CEST): Sensing xenon-host exchange dynamics and binding affinities by NMR, The Journal of Chemical Physics 141 (19) (2014) 194202.

[5] S. Korchak, W. Kilian, L. Mitschang, Degeneracy in cryptophane-xenon complex formation in aqueous solution, Chemical Communications 51 (9) (2015) 1721–1724.

[6] W. Happer, Optical Pumping, Reviews of Modern Physics 44 (2) (1972) 169–249.

[7] G. D. Cates, S. R. Schaefer, W. Happer, Relaxation of spins due to field inhomogeneities in gaseous samples at low magnetic fields and low pressures, Physical Review A 37 (1988) 2877–2885.

[8] T. G. Walker, W. Happer, Spin-exchange optical pumping of noble-gas nuclei, Reviews of Modern Physics 69 (2) (1997) 629–642.

[9] P. Berthault, G. Huber, H. Desvaux, Biosensing using laser-polarized xenon NMR/MRI, Progress in Nuclear Magnetic Resonance Spectroscopy 55 (1) (2009) 35–60.

[10] S. R. Breeze, S. Lang, I. Moudrakovski, C. I. Ratcliffe, J. A. Ripmeester, G. Santyr, B. Simard, I. Zuger, Coatings for optical pumping cells and short-term storage of hyperpolarized xenon, Journal of Applied Physics 87 (11) (2000) 8013–8017.

[11] X. Zeng, E. Miron, W. Van Wijngaarden, D. Schreiber, W. Happer, Wall relaxation of spin polarized ^{129}Xe nuclei, Physics Letters A 96 (4) (1983) 191–194.

[12] N. N. Kuzma, B. Patton, K. Raman, W. Happer, Fast nuclear spin relaxation in hyperpolarized solid ^{129}Xe, Physical Review Letters 88 (2002) 147602.

[13] H. Desvaux, T. Gautier, G. Le Goff, M. Pétro, P. Berthault, Direct evidence of a magnetization transfer between laser-polarized xenon and protons of a cage-molecule in water, The European Physical Journal D - Atomic, Molecular, Optical and Plasma Physics 12 (2) (2000) 289–296.

[14] G. E. Pavlovskaya, Z. I. Cleveland, K. F. Stupic, R. J. Basaraba, T. Meersmann, Hyperpolarized krypton-83 as a contrast agent for magnetic resonance imaging, Proceedings of the National Academy of Sciences 102 (51) (2005) 18275–18279.

[15] Z. I. Cleveland, K. F. Stupic, G. E. Pavlovskaya, J. E. Repine, J. B. Wooten, T. Meersmann, Hyperpolarized ^{83}Kr and ^{129}Xe NMR Relaxation Measurements of Hydrated Surfaces: Implications for Materials Science and Pulmonary Diagnostics, Journal of the American Chemical Society 129 (6) (2007) 1784–1792.

[16] Z. I. Cleveland, G. E. Pavlovskaya, N. D. Elkins, K. F. Stupic, J. E. Repine, T. Meersmann, Hyperpolarized ^{83}Kr MRI of lungs, Journal of Magnetic Resonance 195 (2) (2008) 232–237.

[17] D. M. L. Lilburn, C. Lesbats, J. S. Six, E. Dubuis, L. Yew-Booth, D. E. Shaw, M. G. Belvisi, M. A. Birrell, G. E. Pavlovskaya, T. Meersmann, Hyperpolarized ^{83}Kr magnetic resonance imaging of alveolar degradation in a rat model of emphysema, Journal of The Royal Society Interface 12 (107) (2015) 20150192.

[18] R. K. Mazitov, K. M. Enikeev, A. V. Ilyasov, Magnetic Resonance and Relaxation of Nuclei of Atomic Krypton in Liquid Solutions, Zeitschrift für Physikalische Chemie 155 (Part-1-2) (1987) 55–68.

[19] T. Hughes-Riley, J. S. Six, D. M. Lilburn, K. F. Stupic, A. C. Dorkes, D. E. Shaw, G. E. Pavlovskaya, T. Meersmann, Cryogenics free production of hyperpolarized 129Xe and 83Kr for biomedical MRI applications, Journal of Magnetic Resonance 237 (2013) 23–33.

[20] N. J. Rogers, F. Hill-Casey, K. F. Stupic, J. S. Six, C. Lesbats, S. P. Rigby, J. Fraissard, G. E. Pavlovskaya, T. Meersmann, Molecular hydrogen and catalytic combustion in the production of hyperpolarized ^{83}Kr and ^{129}Xe MRI contrast agents, Proceedings of the National Academy of Sciences 113 (12) (2016) 3164–3168.

[21] A. Nikiel, T. Palasz, M. Suchanek, M. Abboud, A. Sinatra, Z. Olejniczak, T. Dohnalik, G. Tastevin, P.-J. Nacher, Metastability exchange optical pumping of ^{3}He at high pressure and high magnetic field for medical applications, The European Physical Journal Special Topics 144 (1) (2007) 255–263.

[22] P.-J. Nacher, G. Tastevin, X. Maitre, X. Dollat, B. Lemaire, J. Olejnik, A peristaltic compressor for hyperpolarized helium, European Radiology 9 (1999) B18.

[23] K. Suchanek, K. Cieslar, Z. Olejniczak, T. Palasz, M. Suchanek, T. Dohnalik, Hyperpolarized ^{3}He gas production by metastability exchange optical pumping for magnetic resonance imaging;, Optica Applicata 35 (2005) 263–276.

[24] K. H. Andersen, R. Chung, V. Guillard, H. Humblot, D. Jullien, E. Lelièvre-Berna, A. Petoukhov, F. Tasset, First results from Tyrex, the new polarized-3He filling station at ILL, Physica B: Condensed Matter 356 (1) (2005) 103–108.

[25] S. Hiebel, T. Großmann, D. Kiselev, J. Schmiedeskamp, Y. Gusev, W. Heil, S. Karpuk, J. Krimmer, E. Otten, Z. Salhi, Magnetized boxes for housing polarized spins in homogeneous fields, Journal of Magnetic Resonance 204 (1) (2010) 37 – 49.

[26] P. Berthault, H. Desvaux, NMR study of the dissolution of laser-polarized xenon, The European Physical Journal D - Atomic, Molecular and Optical Physics 22 (1) (2003) 65–73.

[27] R. Jiménez-Martínez, D. J. Kennedy, M. Rosenbluh, E. A. Donley, S. Knappe, S. J. Seltzer, H. L. Ring, V. S. Bajaj, J. Kitching, Optical hyperpolarization and NMR detection of ^{129}Xe on a microfluidic chip, Nature Communications 5 (1), (2014).

[28] C. Chauvin, L. Liagre, C. Boutin, E. Mari, E. Léonce, G. Carret, B. Coltrinari, P. Berthault, Note: Spin-exchange optical pumping in a van, Review of Scientific Instruments 87 (1) (2016) 016105.

[29] J. Milani, B. Vuichoud, A. Bornet, P. Miéville, R. Mottier, S. Jannin, G. Bodenhausen, A magnetic tunnel to shelter hyperpolarized fluids, Review of Scientific Instruments 86 (2) (2015) 024101.

[30] S. E. Korchak, W. Kilian, L. Mitschang, Configuration and Performance of a Mobile ^{129}Xe Polarizer, Applied Magnetic Resonance 44 (1-2) (2013) 65–80.

[31] A. S. Kiryutin, B. A. Rodin, A. V. Yurkovskaya, K. L. Ivanov, D. Kurzbach, S. Jannin, D. Guarin, D. Abergel, G. Bodenhausen, Transport of hyperpolarized samples in dissolution-DNP experiments, Physical Chemistry Chemical Physics 21 (25) (2019) 13696–13705.

[32] J. Leggett, R. Hunter, J. Granwehr, R. Panek, A. J. Perez-Linde, A. J. Horsewill, J. McMaster, G. Smith, W. Köckenberger, A dedicated spectrometer for dissolution DNP NMR spectroscopy, Physical Chemistry Chemical Physics 12 (22) (2010) 5883.

[33] K. Kouril, H. Kourilova, S. Bartram, M. H. Levitt, B. Meier, Scalable dissolution-dynamic nuclear polarization with rapid transfer of a polarized solid, Nature Communications 10 (1), (2019).

[34] J. Natterer, J. Bargon, Parahydrogen induced polarization, Progress in Nuclear Magnetic Resonance Spectroscopy 31 (4) (1997) 293 – 315.

[35] K. L. Ivanov, A. N. Pravdivtsev, A. V. Yurkovskaya, H.-M. Vieth, R. Kaptein, The role of level anti-crossings in nuclear spin hyperpolarization, Progress in Nuclear Magnetic Resonance Spectroscopy 81 (2014) 1–36.

[36] D. A. Barskiy, S. Knecht, A. V. Yurkovskaya, K. L. Ivanov, Chemical kinetics and spin dynamics of the formation of hyperpolarization, Progress in Nuclear Magnetic Resonance Spectroscopy 114-115 (2019) 33–70.

[37] T. Theis, M. Truong, A. M. Coffey, E. Y. Chekmenev, W. S. Warren, LIGHT-SABRE enables efficient in-magnet catalytic hyperpolarization, Journal of Magnetic Resonance 248 (2014) 23–26.

[38] A. N. Pravdivtsev, A. V. Yurkovskaya, H.-M. Vieth, K. L. Ivanov, RF-SABRE: A Way to Continuous Spin Hyperpolarization at High Magnetic Fields, The Journal of Physical Chemistry B 119 (43) (2015) 13619–13629.

[39] A. N. Pravdivtsev, I. V. Skovpin, A. I. Svyatova, N. V. Chukanov, L. M. Kovtunova, V. I. Bukhtiyarov, E. Y. Chekmenev, K. V. Kovtunov, I. V. Koptyug, J.-B. Hövener, Chemical Exchange Reaction Effect on Polarization Transfer Efficiency in SLIC-SABRE, The Journal of Physical Chemistry A 122 (46) (2018) 9107–9114.

[40] L. Bordonali, N. Nordin, E. Fuhrer, N. MacKinnon, J. G. Korvink, Parahydrogen based NMR hyperpolarisation goes micro: an alveolus for small molecule chemosensing, Lab on a Chip 19 (3) (2019) 503–512.

[41] N. Amor, P. Zänker, P. Blümler, F. Meise, L. Schreiber, A. Scholz, J. Schmiedeskamp, H. Spiess, K. Münnemann, Magnetic resonance imaging of dissolved hyperpolarized ^{129}Xeusing a membrane-based continuous flow system, Journal of Magnetic Resonance 201 (1) (2009) 93–99.

[42] N. Amor, K. Hamilton, M. Küppers, U. Steinseifer, S. Appelt, B. Blümich, T. Schmitz-Rode, NMR and MRI of Blood-Dissolved Hyperpolarized Xe-129 in Different Hollow-Fiber Membranes, ChemPhysChem 12 (16) (2011) 2941–2947.

[43] B. Niederländer, P. Blümler, T. Brotin, D. Van Dusschoten, A. Offenhäusser, H. J. Krause, W. Heil, Optimized Continuous Application of Hyperpolarized Xenon to Liquids, The Journal of Physical Chemistry A 122 (2018) 9359–9369.

[44] S. Lehmkuhl, M. Wiese, L. Schubert, M. Held, M. Küppers, M. Wessling, B. Blümich, Continuous hyperpolarization with parahydrogen in a membrane reactor, Journal of Magnetic Resonance 291 (2018) 8–13.

[45] M. Roth, P. Kindervater, H.-P. Raich, J. Bargon, H. W. Spiess, K. Münnemann, Continuous ^{1}H and ^{13}C Signal Enhancement in NMR Spectroscopy and MRI Using Parahydrogen and Hollow-Fiber Membranes, Angewandte Chemie International Edition 49 (45) (2010) 8358–8362.

[46] Z. I. Cleveland, H. E. Möller, L. W. Hedlund, B. Driehuys, Continuously Infusing Hyperpolarized ^{129}Xe into Flowing Aqueous Solutions Using Hydrophobic Gas Exchange Membranes, The Journal of Physical Chemistry B 113 (37) (2009) 12489–12499.

[47] Z. I. Cleveland, H. E. Möller, L. W. Hedlund, J. C. Nouls, M. S. Freeman, Y. Qi, B. Driehuys, In Vivo MR Imaging of Pulmonary Perfusion and Gas Exchange in Rats via Continuous Extracorporeal Infusion of Hyperpolarized ^{129}Xe, PLoS ONE 7 (2) (2012) e31306.

[48] A. Causier, G. Carret, C. Boutin, T. Berthelot, P. Berthault, 3d-printed system optimizing dissolution of hyperpolarized gaseous species for micro-sized NMR, Lab on a Chip 15 (9) (2015) 2049–2054.

[49] G. Carret, T. Berthelot, P. Berthault, Enhancing NMR of Nonrelaxing Species Using a Controlled Flow Motion and a Miniaturized Circuit, Analytical Chemistry 89 (5) (2017) 2995–3000.

[50] G. Carret, T. Berthelot, P. Berthault, Inductive Coupling and Flow for Increased NMR Sensitivity, Analytical Chemistry 90 (19) (2018) 11169–11173.

[51] E. Cavallari, C. Carrera, M. Sorge, G. Bonne, A. Muchir, S. Aime, F. Reineri, The ^{13}C hyperpolarized pyruvate generated by ParaHydrogen detects the response of the heart to altered metabolism in real time, Scientific Reports 8 (1), (2018).

[52] J.-B. Hövener, A. N. Pravdivtsev, B. Kidd, C. R. Bowers, S. Glöggler, K. V. Kovtunov, M. Plaumann, R. Katz-Brull, K. Buckenmaier, A. Jerschow, F. Reineri, T. Theis, R. V. Shchepin, S. Wagner, P. Bhattacharya, N. M. Zacharias, E. Y. Chekmenev, Parahydrogen-Based Hyperpolarization for Biomedicine, Angewandte Chemie International Edition 57 (35) (2018) 11140–11162.

[53] F. Shi, A. M. Coffey, K. W. Waddell, E. Y. Chekmenev, B. M. Goodson, Heterogeneous Solution NMR Signal Amplification by Reversible Exchange, Angewandte Chemie International Edition 53 (29) (2014) 7495–7498.

[54] F. Shi, A. M. Coffey, K. W. Waddell, E. Y. Chekmenev, B. M. Goodson, Nanoscale Catalysts for NMR Signal Enhancement by Reversible Exchange, The Journal of Physical Chemistry C 119 (13) (2015) 7525–7533.

[55] K. V. Kovtunov, L. M. Kovtunova, M. E. Gemeinhardt, A. V. Bukhtiyarov, J. Gesiorski, V. I. Bukhtiyarov, E. Y. Chekmenev, I. V. Koptyug, B. M. Goodson, Heterogeneous Microtesla SABRE Enhancement of ^{15}N NMR Signals, Angewandte Chemie International Edition 56 (35) (2017) 10433–10437.

[56] V. V. Zhivonitko, V.-V. Telkki, K. Chernichenko, T. Repo, M. Leskelä, V. Sumerin, I. V. Koptyug, Tweezers for Parahydrogen: A Metal-Free Probe of Nonequilibrium Nuclear Spin States of H_2 Molecules, Journal of the American Chemical Society 136 (2) (2014) 598–601.

[57] K. Sorochkina, V. V. Zhivonitko, K. Chernichenko, V.-V. Telkki, T. Repo, I. V. Koptyug, Spontaneous ^{15}N Nuclear Spin Hyperpolarization in Metal-Free Activation of Parahydrogen by Molecular Tweezers, The Journal of Physical Chemistry Letters 9 (4) (2018) 903–907.

[58] W. Iali, A. M. Olaru, G. G. R. Green, S. B. Duckett, Achieving High Levels of NMR-Hyperpolarization in Aqueous Media With Minimal Catalyst Contamination Using SABRE, Chemistry - A European Journal 23 (44) (2017) 10491–10495.

[59] D. A. Barskiy, L. A. Ke, X. Li, V. Stevenson, N. Widarman, H. Zhang, A. Truxal, A. Pines, Rapid Catalyst Capture Enables Metal-Free *para* -Hydrogen-Based Hyperpolarized Contrast Agents, The Journal of Physical Chemistry Letters 9 (11) (2018) 2721–2724.

[60] P. Miéville, P. Ahuja, R. Sarkar, S. Jannin, P. R. Vasos, S. Gerber-Lemaire, M. Mishkovsky, A. Comment, R. Gruetter, O. Ouari, P. Tordo, G. Bodenhausen, Scavenging Free Radicals To Preserve Enhancement and Extend Relaxation Times in NMR using Dynamic Nuclear Polarization, Angewandte Chemie International Edition 49 (35) (2010) 6182–6185.

[61] A. Kiswandhi, B. Lama, P. Niedbalski, M. Goderya, J. Long, L. Lumata, The effect of glassing solvent deuteration and Gd^{3+} doping on ^{13}C DNP at 5 T, RSC Advances 6 (45) (2016) 38855–38860.

[62] V. V. Zhivonitko, K. Sorochkina, K. Chernichenko, B. Kótai, T. Földes, I. Pápai, V.-V. Telkki, T. Repo, I. Koptyug, Nuclear spin hyperpolarization with ansa-aminoboranes: a metal-free perspective for parahydrogen-induced polarization, Physical Chemistry Chemical Physics 18 (40) (2016) 27784–27795.

[63] P. Niedbalski, A. Kiswandhi, C. Parish, Q. Wang, F. Khashami, L. Lumata, NMR Spectroscopy Unchained: Attaining the Highest Signal Enhancements in Dissolution Dynamic Nuclear Polarization, The Journal of Physical Chemistry Letters 9 (18) (2018) 5481–5489.

[64] X. Ji, A. Bornet, B. Vuichoud, J. Milani, D. Gajan, A. J. Rossini, L. Emsley, G. Bodenhausen, S. Jannin, Transportable hyperpolarized metabolites, Nature Communications 8 (1), (2017).

[65] A. Capozzi, J.-N. Hyacinthe, T. Cheng, T. R. Eichhorn, G. Boero, C. Roussel, J. J. van der Klink, A. Comment, Photoinduced Nonpersistent Radicals as Polarizing Agents for X-Nuclei Dissolution Dynamic Nuclear Polarization, The Journal of Physical Chemistry C 119 (39) (2015) 22632–22639.

[66] A. Capozzi, T. Cheng, G. Boero, C. Roussel, A. Comment, Thermal annihilation of photo-induced radicals following dynamic nuclear polarization to produce transportable frozen hyperpolarized ^{13}C-substrates, Nature Communications 8 (1).

[67] I. Marco-Rius, T. Cheng, A. P. Gaunt, S. Patel, F. Kreis, A. Capozzi, A. J. Wright, K. M. Brindle, O. Ouari, A. Comment, Photogenerated Radical in Phenylglyoxylic Acid for in Vivo Hyperpolarized ^{13}C MR with Photosensitive Metabolic Substrates, Journal of the American Chemical Society 140 (43) (2018) 14455–14463.

[68] S. Kern, L. Wander, K. Meyer, S. Guhl, A. R. G. Mukkula, M. Holtkamp, M. Salge, C. Fleischer, N. Weber, R. King, S. Engell, A. Paul, M. P. Remelhe, M. Maiwald, Flexible automation with compact

NMR spectroscopy for continuous production of pharmaceuticals, Analytical and Bioanalytical Chemistry 411 (14) (2019) 3037–3046.

[69] S. Bowen, C. Hilty, Rapid sample injection for hyperpolarized NMR spectroscopy, Physical Chemistry Chemical Physics 12 (22) (2010) 5766.

[70] B. P. Hills, K. M. Wright, Industrial on-line analysis by nuclear magnetic resonance spectroscopy (Nov. 2002).

[71] J. P. McMullen, K. F. Jensen, Integrated Microreactors for Reaction Automation: New Approaches to Reaction Development, Annual Review of Analytical Chemistry 3 (1) (2010) 19–42.

[72] P. Berthault, H. Desvaux, G. Le Goff, M. Pétro, A simple way to properly invert intense nuclear magnetization: application to laser-polarized xenon, Chemical Physics Letters 314 (1-2) (1999) 52–56.

[73] D. J.-Y. Marion, G. Huber, P. Berthault, H. Desvaux, Effects on ^{1}H and ^{129}Xe NMR spectra of large magnetization created by dissolved laser-polarized xenon, Comptes Rendus Chimie 11 (4-5) (2008) 553–559.

[74] D. J.-Y. Marion, G. Huber, P. Berthault, H. Desvaux, Observation of Noise-Triggered Chaotic Emissions in an NMR-Maser, ChemPhysChem 9 (10) (2008) 1395–1401.

[75] P. Berthault, A. Bogaert-Buchmann, H. Desvaux, G. Huber, Y. Boulard, Sensitivity and Multiplexing Capabilities of MRI Based on Polarized ^{129}Xe Biosensors, Journal of the American Chemical Society 130 (49) (2008) 16456–16457.

[76] N. Eshuis, R. L. E. G. Aspers, B. J. A. van Weerdenburg, M. C. Feiters, F. P. J. T. Rutjes, S. S. Wijmenga, M. Tessari, NMR Trace Analysis by Continuous Hyperpolarization at High Magnetic Field, Angewandte Chemie International Edition 54 (48) (2015) 14527–14530.

[77] L. Frydman, T. Scherf, A. Lupulescu, The acquisition of multidimensional NMR spectra within a single scan, Proceedings of the National Academy of Sciences 99 (25) (2002) 15858–15862.

[78] J.-N. Dumez, Spatial encoding and spatial selection methods in high-resolution NMR spectroscopy, Progress in Nuclear Magnetic Resonance Spectroscopy 109 (2018) 101–134.

[79] L. Frydman, D. Blazina, Ultrafast two-dimensional nuclear magnetic resonance spectroscopy of hyperpolarized solutions, Nature Physics 3 (6) (2007) 415–419.

[80] C. Bretschneider, A. Karabanov, N. C. Nielsen, W. Köckenberger, Conversion of parahydrogen induced longitudinal two-spin order to evenly distributed single spin polarisation by optimal control pulse sequences, The Journal of Chemical Physics 136 (9) (2012) 094201.

[81] L. S. Lloyd, R. W. Adams, M. Bernstein, S. Coombes, S. B. Duckett, G. G. R. Green, R. J. Lewis, R. E. Mewis, C. J. Sleigh, Utilization of SABRE-Derived Hyperpolarization To Detect Low-Concentration Analytes via 1D and 2D NMR Methods, Journal of the American Chemical Society 134 (31) (2012) 12904–12907.

[82] V. Daniele, F.-X. Legrand, P. Berthault, J.-N. Dumez, G. Huber, Single-Scan Multidimensional NMR Analysis of Mixtures at Sub-Millimolar Concentrations by using SABRE Hyperpolarization, ChemPhysChem 16 (16) (2015) 3413–3417.

[83] L. Guduff, D. Kurzbach, C. van Heijenoort, D. Abergel, J.-N. Dumez, Single-Scan ^{13}C Diffusion-Ordered NMR Spectroscopy of DNP-Hyperpolarised Substrates, Chemistry - A European Journal 23 (66) (2017) 16722–16727.

[84] L. Guduff, P. Berthault, C. van Heijenoort, J.-N. Dumez, G. Huber, Single-Scan Diffusion-Ordered NMR Spectroscopy of SABRE-Hyperpolarized Mixtures, ChemPhysChem 20 (3) (2019) 392–398.

[85] S. Ahola, V. V. Zhivonitko, O. Mankinen, G. Zhang, A. M. Kantola, H.-Y. Chen, C. Hilty, I. V. Koptyug, V.-V. Telkki, Ultrafast multidimensional Laplace NMR for a rapid and sensitive chemical analysis, Nature Communications 6 (1), (2015).

[86] J. Zhou, P. C. v. Zijl, Chemical exchange saturation transfer imaging and spectroscopy, Progress in Nuclear Magnetic Resonance Spectroscopy 48 (2-3) (2006) 109–136.

[87] E. Vinogradov, A. D. Sherry, R. E. Lenkinski, From basic principles to applications, challenges and opportunities, Journal of Magnetic Resonance 229 (2013) 155 – 172, frontiers of In Vivo and Materials MRI Research.

[88] L. Schröder, T. J. Lowery, C. Hilty, D. E. Wemmer, A. Pines, Molecular Imaging Using a Targeted Magnetic Resonance Hyperpolarized Biosensor, Science 314 (5798) (2006) 446–449.

[89] N. Tassali, N. Kotera, C. Boutin, E. Léonce, Y. Boulard, B. Rousseau, E. Dubost, F. Taran, T. Brotin, J.-P. Dutasta, P. Berthault, Smart Detection of Toxic Metal Ions, Pb^{2+} and Cd^{2+}, Using a ^{129}Xe NMR-Based Sensor, Analytical Chemistry 86 (3) (2014) 1783–1788.

[90] X. Xu, J.-S. Lee, A. Jerschow, Ultrafast Scanning of Exchangeable Sites by NMR Spectroscopy, Angewandte Chemie International Edition 52 (32) (2013) 8281–8284.

[91] C. Boutin, E. Léonce, T. Brotin, A. Jerschow, P. Berthault, Ultrafast Z-Spectroscopy for ^{129}Xe NMR-Based Sensors, The Journal of Physical Chemistry Letters 4 (23) (2013) 4172–4176.

[92] J. Döpfert, C. Witte, L. Schröder, Fast Gradient-Encoded CEST Spectroscopy of Hyperpolarized Xenon, ChemPhysChem 15 (2) (2014) 261–264.

[93] J. Döpfert, M. Zaiss, C. Witte, L. Schröder, Ultrafast CEST imaging, Journal of Magnetic Resonance 243 (2014) 47–53.

[94] S. Knecht, S. Hadjiali, D. A. Barskiy, A. Pines, G. Sauer, A. S. Kiryutin, K. L. Ivanov, A. V. Yurkovskaya, G. Buntkowsky, Indirect Detection of Short-Lived Hydride Intermediates of Iridium N-Heterocyclic Carbene Complexes via Chemical Exchange Saturation Transfer Spectroscopy, The Journal of Physical Chemistry C 123 (26) (2019) 16288–16293.

[95] N. Bhattacharjee, A. Urrios, S. Kang, A. Folch, The upcoming 3d-printing revolution in microfluidics, Lab Chip 16 (2016) 1720–1742.

[96] S. Waheed, J. M. Cabot, N. P. Macdonald, T. Lewis, R. M. Guijt, B. Paull, M. C. Breadmore, 3d printed microfluidic devices: enablers and barriers, Lab Chip 16 (2016) 1993–2013.

[97] H. Kotturi, A. Abuabed, H. Zafar, E. Sawyer, B. Pallipparambil, H. Jamadagni, M. Khandaker, Evaluation of polyethylene glycol diacrylate-polycaprolactone scaffolds for tissue engineering applications, Journal of Functional Biomaterials 8 (3).

[98] U. Jammalamadaka, K. Tappa, Recent advances in biomaterials for 3d printing and tissue engineering, Journal of Functional Biomaterials 9 (1).

[99] J. R. Choi, K. W. Yong, J. Y. Choi, A. C. Cowie, Recent advances in photo-crosslinkable hydrogels for biomedical applications, BioTechniques 66 (1) (2019) 40–53.

[100] C. Boutin, H. Desvaux, M. Carrière, F. Leteurtre, N. Jamin, Y. Boulard, P. Berthault, Hyperpolarized ^{129}Xe NMR signature of living biological cells, NMR in Biomedicine 24 (10) (2011) 1264–1269.

[101] J. Wolber, A. Cherubini, M. O. Leach, A. Bifone, Hyperpolarized ^{129}Xe NMR as a probe for blood oxygenation, Magnetic Resonance in Medicine 43 (4) (2000) 491–496.

[102] P. Berthault, C. Boutin, Chapter 14:Biosensing and Study of Biological Cells using Hyperpolarized 129Xe, in: Hyperpolarized Xenon-129 Magnetic Resonance, 2015, pp. 261–271.

[103] C. Kjeldsen, J. H. Ardenkjær-Larsen, J. Ø. Duus, Discovery of Intermediates of *lacZ* β-Galactosidase Catalyzed Hydrolysis Using dDNP NMR, Journal of the American Chemical Society 140 (8) (2018) 3030–3034.

[104] J. Eills, E. Cavallari, C. Carrera, D. Budker, S. Aime, F. Reineri, Real Time Nuclear Magnetic Resonance Detection of Fumarase Activity using Parahydrogen-Hyperpolarized [1-13C]fumarate.

[105] E. E. McDonnell, S. Han, C. Hilty, K. L. Pierce, A. Pines, NMR analysis on microfluidic devices by remote detection, Analytical Chemistry 77 (24) (2005) 8109–8114.

[106] M. Mompeán, R. M. Sánchez-Donoso, A. de la Hoz, V. Saggiomo, A. H. Velders, M. V. Gomez, Pushing nuclear magnetic resonance sensitivity limits with microfluidics and photo-chemically induced dynamic nuclear polarization, Nature Communications 9 (1).

[107] L.-S. Bouchard, S. R. Burt, M. S. Anwar, K. V. Kovtunov, I. V. Koptyug, A. Pines, NMR Imaging of Catalytic Hydrogenation in Microreactors with the Use of parahydrogen, Science 319 (5862) (2008) 442–445.

[108] V.-V. Telkki, V. V. Zhivonitko, S. Ahola, K. V. Kovtunov, J. Jokisaari, I. V. Koptyug, http://doi.wiley.com/10.1002/anie.201002685Microfluidic Gas-Flow Imaging Utilizing Parahydrogen-Induced Polarization and Remote-Detection NMR, Angewandte Chemie International Edition 49 (45) (2010) 8363–8366.

[109] J. Eills, W. Hale, M. Sharma, M. Rossetto, M. H. Levitt, M. Utz, High-Resolution Nuclear Magnetic Resonance Spectroscopy with Picomole Sensitivity by Hyperpolarization on a Chip, Journal of the American Chemical Society 141 (25) (2019) 9955–9963.

[110] W. Iali, P. J. Rayner, S. B. Duckett, Using *para* hydrogen to hyperpolarize amines, amides, carboxylic acids, alcohols, phosphates, and carbonates, Science Advances 4 (1) (2018) eaao6250.

[111] M. H. Levitt, Long live the singlet state! , Journal of Magnetic Resonance 306 (2019) 69–74.

[112] M. C. D. Tayler, I. Marco-Rius, M. I. Kettunen, K. M. Brindle, M. H. Levitt, G. Pileio, Direct Enhancement of Nuclear Singlet Order by Dynamic Nuclear Polarization, Journal of the American Chemical Society 134 (18) (2012) 7668–7671.

[113] I. Marco-Rius, M. C. D. Tayler, M. I. Kettunen, T. J. Larkin, K. N. Timm, E. M. Serrao, T. B. Rodrigues, G. Pileio, J. H. Ardenkjaer-Larsen, M. H. Levitt, K. M. Brindle, Hyperpolarized singlet lifetimes of pyruvate in human blood and in the mouse: Hyperpolarized Singlet Lifetimes of Pyruvate *In Vivo*, NMR in Biomedicine 26 (12) (2013) 1696–1704.

[114] W. Iali, S. S. Roy, B. J. Tickner, F. Ahwal, A. J. Kennerley, S. B. Duckett, Hyperpolarising Pyruvate through Signal Amplification by Reversible Exchange (SABRE), Angewandte Chemie International Edition 58 (30) (2019) 10271–10275.

[115] D. R. Glenn, D. B. Bucher, J. Lee, M. D. Lukin, H. Park, R. L. Walsworth, High-resolution magnetic resonance spectroscopy using a solid-state spin sensor, Nature 555 (7696) (2018) 351–354.